STRIPAK complex defects result in pseudosexual reproduction in *Cryptococcus neoformans*

Patricia P. Peterson[1], Sarah Croog[1], Yeseul Choi[1], Sheng Sun[1], and Joseph Heitman[1*]

[1] Department of Molecular Genetics and Microbiology, Duke University Medical Center, Durham, North Carolina, 27710, USA.

* Corresponding author

Email: heitm001@duke.edu (JH)

Keywords: pseudosexual reproduction, PP2A, sexual development, nuclear inheritance, meiosis, phosphatase

Abstract

STRIPAK is an evolutionarily conserved signaling complex that coordinates diverse cellular processes across fungi and animals. In the human fungal pathogen *Cryptococcus neoformans*, STRIPAK was recently shown to play critical roles in maintaining genome stability and controlling both sexual and asexual development. In *Cryptococcus*, sexual reproduction is closely linked to virulence, and our findings demonstrate that the STRIPAK complex plays key roles in both processes. Here, we further investigate the specific roles of the STRIPAK catalytic subunit Pph22 and its regulatory partner Far8 during sexual development. We show that while *pph22*Δ mutants are defective in α-**a** sexual reproduction, exhibiting impaired meiotic progression and a failure to produce viable spores, the deletion of *PPH22* resulted in exclusive pseudosexual reproduction, with progeny inheriting nuclear genomes solely from the wild-type parent. Overexpression of *PPG1*, a related phosphatase, rescued growth and developmental defects in *pph22*Δ mutants, and restored the preference for α-**a** sexual reproduction over pseudosexual reproduction during mating, suggesting functional redundancy within the STRIPAK signaling network. Furthermore, deletion of *FAR8*, another component of the STRIPAK complex, also led to a high rate of pseudosexual reproduction during α-**a** sexual mating, reinforcing the role of STRIPAK in modulating reproductive modes in *C. neoformans*, possibly through regulating nuclear inheritance and meiotic progression. Together, these findings highlight the distinct contributions of STRIPAK to sexual reproduction in *C. neoformans* and suggest that disruptions of this complex affect genome integrity and inheritance mechanisms, with broader implications for fungal adaptation and pathogenesis.

Introduction

In eukaryotic cells, cellular processes are orchestrated by the coordinated activities of protein kinases and phosphatases. Among these, protein phosphatase 2A (PP2A) is a pivotal serine/threonine phosphatase that governs essential functions in cell growth, metabolism, stress responses, proliferation, and differentiation [1-5]. PP2A operates as a heterotrimeric complex, consisting of a scaffold A subunit, a catalytic C subunit, and a regulatory B subunit, which dictates substrate specificity and pathway regulation [6-8]. One key regulatory B subunit is striatin, a core component of the striatin-interacting phosphatase and kinase (STRIPAK) complex, a highly conserved signaling complex that integrates phosphatase and kinase activity to govern developmental and cellular processes across eukaryotes [1, 9-11]. STRIPAK assembly begins with the formation of the PP2A-striatin holoenzyme, which serves as a platform for recruiting additional components to build a larger signaling module [1, 12]. STRIPAK complexes have been identified and characterized in yeasts, filamentous fungi, and mammals, including humans, underscoring their evolutionary conservation. While STRIPAK is broadly conserved across eukaryotes, its functional roles can be context dependent, varying across different organisms and cellular environments [11, 13].

In fungi, STRIPAK is required for both sexual and asexual development, influencing key processes such as cell cycle progression, conidiation, cell fusion, and sporulation [10, 14-17]. In yeasts, STRIPAK-like complexes containing PP2A components are important in the pheromone response pathway and cytokinesis during the sexual cycle [18-20]. In filamentous ascomycetes, STRIPAK homologs have been extensively studied for their roles in sexual and asexual propagation [15, 17, 21-23]. In these species, STRIPAK is essential for the formation of mature fruiting bodies, which are highly complex multicellular structures that arise during sexual reproduction, as well as for asexual growth through conidiation [24, 25]. Similarly, in plant pathogenic fungi such as *Magnaporthe oryzae, Collectrichum graminicola,* and *Fusarium* species, STRIPAK is linked to developmental transitions that enhance virulence, affecting the

ability of these pathogens to infect host tissues [26-29]. More recently, STRIPAK has been characterized in the basidiomycete pathogens *Ustilago maydis* and *Cryptococcus neoformans,* where it plays conserved roles in vegetative growth and sexual reproduction [11, 30]. In *Cryptococcus*, STRIPAK also contributes to genome stability, virulence, and pathogenesis, highlighting its broader significance beyond development.

C. neoformans is a human fungal pathogen in which sexual reproduction has been linked to virulence. Among natural isolates, the α mating type is more prevalent and has been associated with increased virulence, while sexual basidiospores and desiccated yeast cells serve as infectious propagules [31-34]. The dimorphic transition of budding yeast to hyphal growth after mating has also been implicated in pathogenesis, and the formation of sexual structures in environmental niches may enhance fungal survival [35]. Mating between cells of the two opposite mating types, α and **a**, begins with cell-cell fusion, followed by hyphal filamentation, and the formation of a basidium, where nuclear fusion and meiosis occur. After meiosis, nuclei are partitioned into budding spores produced from the basidium, which undergo mitotic division to produce spore chains [36]. Notably, each basidium represents a single meiotic event, and the resulting basidiospores, which form in chains, exhibit distinct adjacent genotypes due to the segregation of alleles during meiosis [37]. This enables the generation of diverse offspring from a single mating event, which may enhance dispersal and dissemination in the environment. Altogether, this sexual cycle contributes not only to genetic diversity but also to environmental persistence and ecological adaptability.

In addition to conventional α-**a** sexual reproduction, *Cryptococcus* can undergo pseudosexual reproduction, an alternative reproductive strategy that results in uniparental nuclear inheritance following mating [38]. Unlike classic meiosis, where both parental nuclei contribute genetic material via recombination to produce haploid progeny, pseudosexual reproduction involves the preferential retention of one parental nucleus while the other is lost or

excluded, leading to meiotic progeny whose nuclear genome is genetically identical to one parent and thus lack meiotic recombination. Mitochondrial uniparental inheritance (UPI) also occurs during this process, with mitochondria preferentially inherited from the *MAT***a** parent [39]. This process shares striking similarities with hybridogenesis, a reproductive mode observed in some animals where hybrid offspring selectively eliminate one parental genome during gametogenesis, ensuring uniparental inheritance in subsequent generations [40]. In *Cryptococcus*, pseudosexual reproduction may facilitate progeny survival and expansion in environments where compatible mating partners are scarce, particularly when high genetic divergence or karyotype variation limits traditional mating. Despite its potential role in adaptation and persistence, the molecular mechanisms underlying this process, and the genetic factors involved, remain largely unknown.

In this study, we investigated the roles of Pph22 and Far8, two key components of the STRIPAK complex, which are critical for *C. neoformans* sexual development. Genotyping and whole-genome sequencing of progeny from *pph22*Δ × wild-type crosses revealed that reproduction occurs exclusively through pseudosexual reproduction, with uniparental nuclear inheritance derived solely from the wild-type parent. Fluorescence microscopy further demonstrated that while *pph22*Δ nuclei can migrate into the basidium and initiate meiosis, they fail to generate viable spores, implicating *PPH22* in meiotic progression. Additionally, overexpression of *PPG1*, a functionally related phosphatase, suppressed defects in vegetative growth, stress responses, and sexual growth caused by loss of *PPH22*, highlighting potential compensatory mechanisms within the STRIPAK network. Notably, we found that pseudosexual reproduction also occurs at a high rate in *far8*Δ mutant x wild type crosses, further supporting a role for STRIPAK in coordinating nuclear inheritance and meiotic processes. These findings establish STRIPAK as a key regulatory network in *Cryptococcus* reproduction and suggest that disruptions to this complex may broadly influence genetic stability and inheritance mechanisms in this fungal pathogen.

Results

*pph22*Δ mutants exhibit reduced mating efficiency and abnormal sexual structures

We previously showed that deletion of *PPH22* causes severe mating defects during α-**a** sexual reproduction, as well as in a self-fertile α/**a** diploid strain, leading to significantly delayed sexual development [30]. To further investigate the dynamics of *pph22*Δ mutants during mating, *pph22*Δ strains were crossed with a wild-type partner of the opposite mating type and incubated on MS medium. To overcome the growth defects of *pph22*Δ on nutrient-limited MS media, mating was facilitated by pre-growing mutant cells before adding a smaller amount of wild-type cells, as described previously [30]. After six weeks of incubation, wild-type crosses displayed extensive hyphal growth, basidia formation, and basidiospore production. In contrast, *pph22*Δ x wild type mating patches showed only limited signs of sexual development (Fig 1A). Most patches lacked visible sexual structures, though occasional hyphae and basidia were observed. Basidia were often bald or produced few spores, and many spores appeared collapsed rather than forming the elongated spore chains characteristic of wild-type mating.

To observe morphological differences in sexual structures between *pph22*Δ and wild-type crosses at a higher resolution, scanning electron microscopy (SEM) of the mated strains was performed. In *pph22*Δ x wild type crosses, many basidia terminating from the end of a hyphal branch were considerably rounded and enlarged compared to the wild-type cross and did not produce spores (Fig 1B). When spores were observed, they often had a collapsed appearance, similar to what was seen by light microscopy (Fig 1A). During α-**a** sexual reproduction in the wild type x wild type cross, the clamp cells, which are critical for faithful segregation of nuclei in the dikaryotic hyphae [41, 42], were fused to the subapical cell in the elongating hyphal branch. In mated *pph22*Δ x wild type, both fused and unfused clamp cells could be observed along the same hypha, suggesting a potential defect in nuclear distribution or clamp cell fusion. Due to the observed defects in mating, we quantified cell–cell fusion frequency by incubating crosses between *pph22*Δ*::NAT* and wild type::*NEO* strains on MS

127 medium for three days. After incubation, cells were harvested and plated on YPD supplemented
128 with either NAT, NEO, or both NAT and NEO. Crosses between wild type::*NAT* and wild
129 type::*NEO* strains were included as a control. Fusion events were quantified by counting colony-
130 forming units (CFUs) on YPD+NAT+NEO plates, which represent dual-resistant fusion products.
131 Fusion frequency was calculated as the number of CFUs on YPD+NAT+NEO divided by the
132 sum of CFUs on YPD+NAT and YPD+NEO, representing the total recovered population. A
133 significant reduction in fusion frequency was observed in *pph22*Δ**a** × WTα and *pph22*Δα × WT**a**
134 crosses compared to the wild-type control (Fig S1A). There was a significant reduction in cell-
135 cell fusion frequency in *pph22*Δ**a** x WTα and *pph22*Δα x WT**a** crosses (5.1% to 5.7% of WT x
136 WT). Taken together, these results suggest that *PPH22* is critical for α-**a** sexual mating and
137 proper sexual development.
138
139 **Progeny from *pph22*Δ x wild type crosses are produced exclusively through**
140 **pseudosexual reproduction**
141 To further investigate the reproductive mode of *pph22*Δ x WT crosses, spores were
142 dissected from individual basidia for phenotypic and genotypic analysis. *pph22*Δ mutant strains
143 have severe growth defects and form significantly smaller colonies compared to wild type.
144 Germinated spores from *pph22*Δ x WT formed colonies that were fast growing and uniform in
145 size on YPD (Fig S1B). Streaking onto YPD and YPD+NAT (selecting for the *pph22*Δ*::NAT*
146 mutation) showed that all dissected spores were NAT-sensitive, indicating the absence of
147 *pph22*Δ mutants among the recovered progeny, potentially suggesting that the spores originated
148 from unisexual reproduction of the wild-type parental strain [43]. To investigate this possibility,
149 spores were dissected from basidia of two independent *pph22*Δ**a** × WTα crosses and one
150 *pph22*Δα × WT**a** cross to yield viable progeny. PCR genotyping of the *STE20* gene in the
151 mating-type locus *(MAT*) revealed that all progeny from each individual basidium contained
152 either the *MAT***a** or the *MAT*α allele, which strictly corresponded to the allele from the wild-type

153 parent (Table 1, Fig S1C). PCR of the *COX1* gene also indicated that the mitochondria was
154 predominantly inherited from the *MAT***a** parent, consistent with mitochondrial uniparental
155 inheritance (mito-UPI) in *Cryptococcus* [39, 44]. *MAT*α mitochondrial inheritance was observed
156 in *pph22*Δ**a** × WTα crosses at a frequency of 32% (7 out of 22 basidia), which is higher than the
157 expected frequency of *MAT*α mitochondria leakage of around 5% to 10% [45]. However, six of
158 these basidia originated from the same mating spot, leaving open the possibility that the
159 inherited *MAT*α mitochondria in the progeny resulted from a single mating event. Similarly, in
160 random spore dissection, 15 out of 65 germinated progeny possessed *MAT*α mitochondria, but
161 were dissected from a single mating spot. It is unclear whether the *pph22*Δ mutation leads to
162 increased *MAT*α mitochondrial inheritance. These results suggest that progeny from *pph22*Δ ×
163 WT inherited only the wild-type parental nuclei. Additionally, the presence of mitochondria from
164 the *MAT***a** parent in *MAT*α progeny indicates that these progeny are not the result of unisexual
165 reproduction. These observations demonstrate that the mode of reproduction in *pph22*Δ × WT
166 crosses is pseudosexual, during which cells of the opposite mating type fuse but the nuclear
167 content of only one parental nucleus is transmitted to the progeny [38].

168 Following PCR genotyping assays, whole-genome sequence analysis was conducted to
169 determine if there was any evidence of meiotic recombination in the F1 progeny from *pph22*Δ**a**
170 × WTα. The *pph22*Δ strains utilized in this study were obtained from dissection of a KN99**a**/α
171 *PPH22/pph22*Δ heterozygous diploid mutant and are congenic with H99 [30, 46]. Besides the
172 mating-type locus on chromosome 5, there are two other genomic regions on chromosomes 11
173 and 14 that differ between H99α and KN99**a** background strains [47, 48]. Twelve progeny from a
174 single basidia (Table 1, spot D basidium 1) were subjected to Illumina whole-genome
175 sequencing and reads were aligned to the H99α reference genome for variant calling and SNP
176 analysis (Fig 2). The KN99**a** *pph22*Δ parental strain and the KN99**a**/α diploid strain (CnLC6693)
177 from which it was derived served as controls. Variant analysis confirmed that only the H99α
178 nuclear genome was inherited in the progeny, as evidenced by the absence of SNPs at the

179 indicated polymorphic loci. Alignment of reads from the KN99 parental strains and progeny to
180 the H99α mitochondrial genome also confirmed the presence of the intron in the KN99**a** *COX1*
181 gene, supporting the results from PCR genotyping. Collectively, the lack of meiotic
182 recombination supports that the progeny from mating of *pph22*Δ × WT arose through a
183 pseudosexual reproductive process and not via α-**a** sexual reproduction.
184
185 **Uniparental nuclear inheritance observed after mating via fluorescence microscopy**
186 Previous studies with fluorescently marked nuclei provided evidence that pseudosexual
187 reproduction in *Cryptococcus* results from loss of one parental nucleus during hyphal branching
188 following mating [38]. A similar approach was taken to investigate nuclear migration during
189 mating in *pph22*Δ × WT crosses. The gene encoding the nucleolar protein Nop1 was fused with
190 GFP or RFP (mCherry) and introduced ectopically into the safe haven region of *pph22*Δ**a**
191 (*NOP1-GFP-NEO)*, KN99**a** (*NOP1-GFP-NEO)*, and H99α (*NOP1-mCherry-HYG*) [49].
192 Homologous recombination at the target locus was confirmed by PCR genotyping. *pph22*Δ and
193 KN99**a** strains expressing Nop1-GFP were crossed with H99α expressing Nop1-RFP on MS
194 media and monitored for signs of mating (Fig S2A). In wild-type crosses, live-cell imaging
195 revealed hyphae containing both GFP- and RFP-tagged proteins following cell-cell fusion,
196 maintaining a stable dikaryotic state throughout hyphal elongation and branching, with green
197 and red fluorescent signals overlapping or appearing in close proximity (Fig S2B). In the basidial
198 heads, the final stages of the sexual cycle were observed, including karyogamy, where the two
199 parental nuclei fused, followed by meiosis and subsequent inheritance of fluorescent tags from
200 both parents in the haploid basidiospores. In total, 27 basidia from two independent crosses
201 were observed to produce spores that contained both fluorescent markers.
202 Nuclear dynamics in *pph22*Δ crosses were notably distinct from those in wild-type
203 crosses. As expected, *pph22*Δ**a** x H99α exhibited decreased mating efficiency, but spore
204 production was still observed after six to eight weeks of incubation (Fig S2A). Fluorescence

205 imaging showed that both red and green nuclear markers initially coexisted within the same
206 hyphal compartment and could be tracked along the elongating hyphal branch. However, at
207 certain branch points, the green *pph22*Δ nucleus was selectively lost, allowing only the red wild-
208 type nucleus to undergo meiosis in the terminating basidium (Fig S2C). Among 40 basidia
209 analyzed from four independent crosses, 15 did not produce spores. Of these, 12 displayed
210 both red and green signals in the basidium head, while the remaining three showed only the red
211 signal. The other 25 basidia successfully produced spores, with 20 containing only the signal
212 from the wild-type parent. This finding aligns with previous work suggesting that hyphal
213 branching may facilitate nuclear exclusion, which can be followed by endoreplication and
214 meiosis of the retained nucleus [38].

215 In contrast, there were also cases in crosses of *pph22*Δ x WT where the wild-type
216 nucleus was lost following hyphal branching, after which the resulting sexual structures
217 exhibited abnormal morphology (Fig 3). Several observations suggested that, after the loss of
218 the red wild-type signal in a hyphal branch, the green *pph22Δ* nucleus could undergo
219 endoreplication followed by nuclear division, resulting in two green nuclei within a single hyphal
220 compartment, indicating a mechanism by which a dikaryotic-like state could be reestablished
221 (Figure 3A). There were also instances where, following wild-type nuclear exclusion, only the
222 *pph22*Δ fluorescent signal was inherited in the basidiospores, which appeared collapsed onto
223 the basidium head (Fig 3B, 3C). Notably, five basidia that produced spores exhibited only the
224 green signal in the progeny., suggesting that the *pph22*Δ mutant nucleus is capable of migrating
225 into the basidium, undergoing diploidization, and potentially entering the meiotic process.
226 However, despite this apparent progression, the consistent inability to recover *pph22*Δ mutant
227 progeny from any dissection of *pph22*Δ x WT crosses, indicates a meiotic or post-meiotic defect
228 that prevents successful germination. There was also evidence that maintenance of only the
229 *pph22*Δ nucleus negatively impacted hyphal morphology, significantly altering both the shape

230 and structure (Fig 3D). Additionally, in another hyphal branch, there were two nuclei detected for
231 each color to yield four nuclei in individual cells, suggesting a failure in nuclear sorting or
232 segregation following DNA replication. Together with spore genotyping analyses, these findings
233 suggest that: 1) pseudosexual reproduction may occur through the loss of one parental nucleus
234 during hyphal branching and 2) the *pph22*Δ mutation disrupts normal sexual development,
235 including nuclear migration, hyphal morphology, and sporulation.
236
237 **α-a sexual reproduction can be restored in *pph22*Δ *suppressor* mutants**
238 *pph22*Δ strains can accumulate spontaneous suppressor mutations that restore mating,
239 hyphal growth, basidia production, and sporulation nearly to the wild-type level (Fig 4A) [30]. To
240 determine if the *pph22*Δ *suppressor* (*sup)* mutant strains could also suppress pseudosexual
241 reproduction, F1 progeny from *pph22*Δ *sup* x WT crosses were analyzed. In one such cross,
242 germinated spores containing the *NAT* drug-resistance marker were recovered during
243 dissection, in contrast to strictly NAT-sensitive *pph22*Δ x WT progeny, providing evidence the
244 suppressor mutation could restore *pph22*Δ spore viability following α-**a** sexual mating, although
245 the resulting colonies were notably smaller in size (Fig 4B). The frequency of *pph22*Δ::*NAT*
246 among the progeny was 45%, consistent with the expected segregation of a single selectable
247 allele. However, in crosses with two other independently derived *pph22*Δ *sup* strains, no NAT
248 resistant progeny were recovered, suggesting incomplete suppression of *pph22*Δ mutant
249 defects following mating in those strains.
250 We next investigated mating type and mitochondrial genome segregation in *pph22*Δ *sup*
251 x WT crosses. All *pph22*Δ *sup* isolates that were obtained in our previous study possess the
252 *MAT*α allele and therefore were crossed with KN99**a**. This led to a complication in using the
253 same PCR genotyping strategy to determine how the mitochondria was inherited in the progeny
254 from these crosses, as KN99**a** and KN99α background strains have identical mitochondria
255 genomes. Therefore, *pph22*Δ *sup* strains were crossed with the KN99**a** strain SSH118, which

256 carries a recombinant mitochondrial genome, and restriction fragment length polymorphism
257 (RFLP) analysis was used to identify the parental source of the mitochondrial genome in the
258 progeny (Fig 4C, S3). In each *pph22*Δ *sup* x WT cross, each basidium that was dissected came
259 from different mating spots, so that the progeny analyzed were the result of independent mating
260 events. The *MAT* allele was determined through PCR genotyping of the *STE20* gene, as in
261 previous experiments, and mitochondrial type was identified through PCR amplification of *COX1*
262 followed by BsrI digestion and RFLP analysis (Fig S3B, S3C, S3D). In two independent crosses,
263 both **a** and α mating types were found among the genotyped basidia and, interestingly, many
264 progeny were heterozygous for the *MAT* allele (Fig 4C, S3E). However, in a third independent
265 cross with a different *pph22*Δ *sup* strain, only progeny of one mating type were recovered,
266 consistent with pseudosexual reproduction. The fact that progeny exhibiting *MAT* heterozygosity
267 also came from basidia with high germination rates suggests that this cannot be explained by
268 aneuploidy alone, as an imbalance in chromosome number in aneuploid spores would lead to
269 reduced germination rates.
270 Flow cytometry analysis of progeny heterozygous for the *MAT* locus revealed that
271 increased DNA content correlated with the presence of the *pph22*Δ*::NAT* deletion allele (Fig
272 S3F). Specifically, NAT-sensitive progeny remained haploid, while all NAT-resistant progeny
273 displayed peaks at 1N, 2N, and 4N, suggesting altered DNA replication or disrupted ploidy
274 regulation in these cells. These results suggest that *PPH22* may have a role in ploidy regulation,
275 and its loss may disrupt cell cycle regulation and lead to altered DNA inheritance patterns.
276 Further analysis, such as whole-genome sequencing, could help clarify which process may be
277 maintaining *MAT* heterozygosity in the NAT-sensitive progeny. While mitochondria in the
278 majority of progeny were inherited from the *MAT***a** parent, progeny from two out of seven basidia
279 from independent mating spots in one of the *pph22*Δ *sup* x WT crosses inherited mitochondria
280 from the *MAT*α parent (Fig S3E). Together, with the genotyping results from *pph22*Δ x WT
281 crosses, these findings suggest that deletion of *PPH22* may also influence mitochondrial

282 inheritance. Although no evidence of pseudosexual reproduction was found in the *pph22*Δ *sup*
283 crosses, the observed α-**a** sexual reproduction was atypical, characterized by an unexpected
284 segregation of mating-type alleles.
285
286 **Overexpression of *PPG1* suppresses loss of *PPH22***
287 All independently obtained *pph22*Δ *sup* mutant strains were found to be aneuploid for a
288 segment of chromosome 6 encompassing seven genes [30]. Of these genes, *PPG1*, which
289 encodes a putative PP2A catalytic subunit and shares significant sequence similarity with
290 Pph22, was overexpressed 40-fold in the *pph22*Δ *sup* mutants compared to wild type [30]. To
291 determine if *PPG1* overexpression was the causative mutation suppressing *pph22*Δ
292 phenotypes, a *PPG1* allele with a constitutively active promoter (P_{TEF1}-*PPG1-NEO)* was
293 integrated into the safe haven 1 of the *PPH22/pph22*Δ heterozygous mutant diploid strain and
294 homologous recombination was confirmed through PCR genotyping. Following self-
295 filamentation on MS media, random spores were dissected and germinated on YPD (Fig 5A).
296 Colonies containing both *NAT* and *NEO* drug resistance markers, confirmed by growth on
297 selective media and PCR genotyping, were faster growing and larger in size than *pph22*Δ
298 mutant colonies, suggesting that overexpression of *PPG1* can partially rescue growth defects of
299 *pph22*Δ.
300 Next, to examine the role of *PPG1* overexpression in response to different nutrient and
301 stress conditions, *pph22*Δ *PPG1-OE*, *pph22*Δ, *pph22*Δ *sup, ppg1*Δ, and wild type strains were
302 serially diluted and spotted onto YPD at 25ºC, 30ºC, and 37ºC; YPD with 1 M sorbitol; YPD with
303 rapamycin; and YPD with the immunosuppressive drugs FK506 or cyclosporine A (CsA) (Fig
304 5B). *pph22*Δ exhibited severe growth defects or no growth on YPD at 25ºC, 30ºC, and 37ºC, as
305 well as on YPD supplemented with sorbitol, FK506, or cyclosporine A, which was partially
306 reversed in the *pph22*Δ *sup* strain, consistent with previously published results. On YPD
307 supplemented with rapamycin, on which *pph22*Δ strains do not have noticeable defects

308 compared to wild type, both *pph22*Δ *sup* and *pph22*Δ *PPG1-OE* strains displayed significant
309 growth advantages. Collectively, overexpression of *PPG1* in the *pph22*Δ mutant was able to fully
310 restore or nearly restore growth to wild-type levels under each condition tested, suggesting that
311 P_{TEF1}-*PPG1* is more effective at compensating for *pph22*Δ than overexpression of *PPG1* due to
312 aneuploidy in *pph22*Δ *sup* strains.

313 It was surprising that *ppg1*Δ did not phenocopy *pph22*Δ, and only exhibited growth
314 defects on YPD at 25ºC and on YPD supplemented with sorbitol or rapamycin, compared to
315 growth on YPD at 30ºC. In fact, *ppg1*Δ displayed similar growth to *pph22*Δ *PPG1-OE* under
316 several conditions, including growth at 30ºC and 37ºC as well as in the presence of FK506 and
317 CsA. These results suggest that while Pph22 and Ppg1 are hypothesized to have similar
318 functions and may play partially compensatory roles, Pph22 is likely the primary catalytic
319 subunit of PP2A, as its loss leads to more severe effects than the loss of *PPG1.* To assess the
320 abilities of *ppg1*Δ and *pph22*Δ *PPG1-OE* strains to produce melanin pigment and
321 polysaccharide capsule, important virulence factors to protect cells from the host immune
322 response during *Cryptococcus* infection. To induce melanin and capsule production, cells were
323 grown on Niger seed agar and in RPMI media, respectively, with both incubated at 30ºC.
324 *pph22*Δ *sup* and *pph22*Δ *PPG1-OE* produced similar amounts of melanin and were comparable
325 to the wild type, while *ppg1*Δ could not produce melanin, similar to the *lac1*Δ negative control
326 (Fig 5C). These results suggest that *PPG1* is required for melanin production, while *PPG1*
327 overexpression in the *pph22*Δ background is sufficient to restore this virulence trait. India ink
328 counterstaining of RPMI-grown cells showed that *PPG1* overexpression restored normal cell
329 morphology in the *pph22*Δ mutant, though capsule production was still impaired (Fig 5D). In
330 contrast, *ppg1*Δ cells could produce capsule, albeit to a lesser extent than wild-type cells.
331 Together, these findings are consistent with the idea that *PPG1* can functionally compensate for
332 the loss of *PPH22* in certain contexts.

333 To further explore the functional differences between Pph22 and Ppg1, 3D structural
334 models of the STRIPAK complex with either Pph22 or Ppg1 as the catalytic subunit were
335 generated with AlphaFold3 [50]. The resulting Pph22-containing structure was comparable to
336 the previously published model generated with AlphaFold2, though slight differences in folding
337 were observed [30, 51]. The two models appeared largely similar, indicating that Ppg1 can
338 potentially assemble into a complex with the other STRIPAK subunits (Fig S4A, S4B). Cryo-EM
339 studies of the human STRIPAK complex have demonstrated that Far8 forms a homotetramer,
340 serving as a scaffold at the base of the complex [12]. To assess whether *Cryptococcus* Far8
341 could similarly assemble into a tetramer, a structural model was generated using four copies of
342 the Far8 protein (Fig S4C). This model was then combined with either the Pph22-Tpd3 or Ppg1-
343 Tpd3 heterodimers to examine PP2A assembly. Both models appeared highly similar overall,
344 though the four Far8 proteins adopted slightly different conformations in each structure (Fig
345 S4D, S4E). These findings suggest that both Pph22 and Ppg1 can potentially integrate into
346 STRIPAK in a comparable manner, perhaps filling analogous roles within the complex.

347 Finally, the involvement of Ppg1 during mating was examined by crossing *ppg1*Δ and
348 *pph22*Δ *PPG1-OE* strains with wild type. Similar to what has been observed in *pph22*Δ crosses,
349 *ppg1*Δ x WT exhibited delayed mating and hyphae were produced only in isolated spots on the
350 mating patch after six weeks of incubation (Fig 5E compared to Fig 1A). With further incubation,
351 more extended hyphal branches were produced but mostly bald basidia heads with almost no
352 spore formation. In contrast, *pph22*Δ *PPG1-OE* x WT crosses displayed signs of mating at a
353 similar rate to wild type and produced abundant basidia with spore chains (Fig 5E compared to
354 Fig 4A). These findings indicate that Ppg1 plays a crucial role during mating and sexual
355 development, similar to Pph22. Taken together, this further supports the conclusion that *PPG1*
356 overexpression is the key mutation suppressing *pph22*Δ, as targeted overexpression of *PPG1* in
357 the *pph22*Δ background similarly restored both mating and growth deficiencies.

358 **Pseudosexual reproduction also occurs at a high rate in *far8*Δ mutant crosses**

359 It has been reported that pseudosexual reproduction occurs at a rate of ~1% between
360 wild-type mating partners with compatible parental genomes, as well as in partners with
361 incompatible parental genomes due to genetic divergence or genome structure variation [38,
362 52]. The analyses presented here demonstrated that deletion of *PPH22* results in exclusively
363 pseudosexual reproduction following α-**a** sexual mating. To further investigate whether other
364 mutations in the STRIPAK complex influence pseudosexual reproduction, *far8*Δ mutant crosses
365 were analyzed. Far8 has also been shown to be critical during *Cryptococcus* sexual
366 development, with *far8*Δ strains exhibiting severe defects in hyphal production and sporulation.
367 To inspect the sexual structures of *far8*Δ x WT crosses in higher resolution, hyphae, basidia,
368 and spore chains were imaged with SEM (Fig 6A). Spores were observed budding from the
369 basidia in irregular numbers, often exceeding the typical set of four. In some cases, seven or
370 more spores emerged independently from separate sites on a single basidium. *far8*Δ strains
371 have been predominantly identified as diploid, suggesting that mating could result in triploid
372 meiosis. This raises the possibility that the observed irregular spore structures may be
373 influenced by the unique genomic composition in the basidium.

374 Next, spores were dissected from individual basidia from both *far8*Δ **a** x WTα and *far8*Δ
375 α x WT**a** crosses. Spores that germinated formed mostly homogenously sized colonies on YPD
376 and did not contain the drug resistance marker, but occasionally small, slow-growing *far8*Δ
377 mutant colonies were obtained (Fig 6B). In total, spores from 16 basidia obtained from nine
378 independent mating spots were dissected and genotyped (Fig 6C). Given the genomic instability
379 of triploid meiosis, reduced spore viability was expected. However, surprisingly, 10 out of 16
380 basidia exhibited germination rates above 70%, with an overall average of 79%, which is
381 comparable to the germination rate observed in progeny from wild-type crosses. PCR
382 genotyping of the *MAT* locus and mitochondrial DNA in progeny from 11 out of 16 dissected
383 basidia were consistent with pseudosexual reproduction, characterized by uniparental nuclear

384 inheritance from only the wild-type parent, a pattern also observed in *pph22*Δ mutant crosses,
385 and mitochondrial inheritance from the *MAT***a** parent. Heterozygosity at the *MAT* locus was also
386 detected in some progeny from the remaining five basidia of the *far8*Δ x WT crosses,
387 resembling the findings in the *pph22*Δ *sup* x WT crosses. Notably, 11 out of 16 progeny
388 possessing both *MAT***a** and *MAT*α also had the *far8*Δ mutant allele, which may be attributed to
389 the altered genomic structure of the *far8*Δ parental strains. Taken together, these results
390 suggest that loss of STRIPAK components *PPH22* or *FAR8* drives pseudosexual reproduction,
391 with the mutant nuclei at a selective disadvantage to the wild-type nucleus, as shown by
392 uniparental nuclear inheritance predominantly from the wild-type parent across multiple
393 independent crosses (Fig S5).

394 **Discussion**

395 The STRIPAK complex has been broadly recognized across fungi as a critical regulator
396 of both asexual and sexual development. In *C. neoformans*, we previously demonstrated that
397 mutants defective in STRIPAK components exhibit defects in several developmental processes,
398 along with increased genome instability, leading to segmental and whole-chromosome
399 duplications or losses [30]. Additionally, STRIPAK mutations were shown to impact the
400 production of virulence traits and pathogenesis during infection. In this study, we further
401 explored the specific roles of STRIPAK during mating and sexual development, identifying two
402 genes, *PPH22* and *FAR8*, that were directly involved in pseudosexual reproduction. This
403 unusual reproductive strategy, which was previously characterized in our lab, occurs when there
404 is incompatibility between mating partners due to genetic divergence or genome structure
405 variation, allowing *C. neoformans* to overcome reproductive barriers [38]. While previously
406 predicted to occur at low frequencies, pseudosexual reproduction enables the production of
407 viable offspring in conditions where successful α-**a** sexual reproduction is not possible or is
408 inefficient, contributing to survival and adaptation.

409 It has been hypothesized that pseudosexual reproduction may preferentially favor the
410 predominance of one mating type over the other and that specific factors influence which
411 nucleus is selectively lost following mating. Our findings provide evidence for genetic factors
412 influencing pseudosexual reproduction, as progeny from crosses involving *pph22*Δ or *far8*Δ
413 mutants exclusively inherited their nuclear genome from the wild-type parent. This supports the
414 hypothesis that, even in cases where mating partners are genetically compatible, intrinsic gene
415 variation can endow one genome with a selective advantage over the other. Such selective
416 inheritance could potentially contribute to fungal adaptation, as it might allow for the retention of
417 beneficial genetic traits while discarding less advantageous ones. Given that loss of *PPH22* or
418 *FAR8* leads to widespread genome instability, including segmental and whole chromosomal
419 aneuploidy, it is likely that these defects impose a fitness cost during sexual development,

420 favoring the retention of the more stable wild-type genome. The defective spore formation
421 observed in *pph22*Δ and *far8*Δ mutants, along with the presence of aberrant DNA content in the
422 progeny, suggests that these mutations may impair proper chromosome segregation or meiotic
423 progression. As a result, selective nuclear retention in pseudosexual reproduction may serve as
424 a mechanism to safeguard genomic integrity, ensuring that only nuclei with fewer deleterious
425 mutations or with more favorable genomic configurations contribute to the next generation.

426 During *Cryptococcus* sexual development, the process of nuclear migration, segregation
427 of nuclei within dikaryotic hyphae, and meiosis are tightly coordinated processes that ensure
428 proper exchange and inheritance of genetic material [34, 53]. STRIPAK has been implicated in
429 actin cytoskeletal organization in other organisms, raising the possibility that its components
430 may play a role in regulating nuclear dynamics during mating [18, 54-57]. In *Cryptococcus*,
431 sexual reproduction involves an extended dikaryotic phase prior to karyogamy, requiring precise
432 nuclear positioning within hyphae. Our fluorescence microscopy data indicate that *pph22*Δ
433 mutants exhibit nuclear segregation defects, as their nuclei frequently fail to reach the basidium.
434 This suggests that *PPH22* may be required for proper nuclear migration during hyphal
435 branching and elongation. However, the observation that wild-type nuclei were sometimes lost
436 without generating viable *pph22*Δ spores suggests that *PPH22* also plays a direct role in
437 meiosis. These findings highlight the role of STRIPAK components in maintaining nuclear
438 integrity throughout sexual development.

439 Interestingly, although recessive mutations are typically complemented in a dikaryon by
440 the presence of a wild-type allele in the opposing nucleus, these findings provide additional
441 evidence that *pph22* mutations are haploinsufficient in this context. Developmental defects were
442 observed in dikarya formed between *pph22*Δ and wild-type strains, and importantly, it was
443 previously demonstrated that a *PPH22/pph22*Δ heterozygous diploid is haploinsufficient,
444 supporting the conclusion that a single copy of *PPH22* is insufficient to support normal

445 development in a diploid or dikaryon. This dosage sensitivity may in part explain the dominance
446 of the wild-type genome in pseudosexual reproduction. Additionally, frequent aneuploidy
447 observed in the *pph22*Δ mutant strains may further compromise nuclear division and migration
448 or meiotic progression, contributing to the nuclear selection bias. Together, these data suggest
449 that both haploinsufficiency and genomic instability may underlie the strong inheritance bias and
450 disrupted sexual development seen in *pph22*Δ crosses, potentially serving as a mechanism to
451 eliminate defective nuclei and maintain genome integrity.

452 The relationship between *PPH22* and *PPG1* suggests functional redundancy, as
453 overexpression of *PPG1* can compensate for *pph22*Δ during both vegetative growth and sexual
454 development. This compensation indicates that *PPG1* can partially fulfill the role of *PPH22* in
455 regulating key cellular processes, likely due to their structural and functional similarities.
456 However, despite this redundancy, *PPH22* appears to have a more critical role, as *ppg1*Δ
457 mutants exhibited more subtle phenotypes compared to the severe defects observed in *pph22*Δ.
458 Notably, while deletion of *PPH22* is synthetically lethal with calcineurin inhibition by FK506 or
459 cyclosporine A, deletion of *PPG1* did not cause a significant growth defect under these
460 conditions. This suggests that *PPH22* plays a predominant role in maintaining essential
461 phosphatase activity that becomes indispensable when calcineurin is inhibited, whereas *PPG1*
462 may function as a secondary phosphatase with limited capacity to support survival under these
463 stresses. These findings reinforce the idea that *PPH22* is the primary catalytic subunit of PP2A,
464 with *PPG1* providing only partial redundancy. This difference in phenotypic severity highlights
465 the distinct regulatory contributions of these phosphatases, with *PPH22* playing a dominant role
466 in STRIPAK-dependent processes.

467 Overall, our findings highlight the critical role of the STRIPAK complex in coordinating
468 key aspects of *Cryptococcus* sexual reproduction and development, including nuclear dynamics
469 during mating, genome stability, and meiotic progression. While STRIPAK has been implicated

470 in developmental processes across diverse fungal species, its role in pseudosexual
471 reproduction is intriguing and unique to *Cryptococcus,* where it seems to bear a resemblance to
472 hybridogenesis observed in some animal species. The ability to selectively retain one parental
473 nucleus during mating may serve as a mechanism to maintain genome integrity in the face of
474 genetic instability, ensuring the production of viable progeny when conventional mating
475 pathways are disrupted. Our study provides new insights into the genetic factors that govern
476 sexual reproduction in *Cryptococcus*, shedding light on how STRIPAK complex mutations
477 influence nuclear selection and inheritance. Future studies will explore how STRIPAK
478 coordinates with other signaling pathways, such as calcineurin and MAPK regulation, to direct
479 cellular growth processes. Additionally, investigating whether similar mechanisms operate in
480 other fungal pathogens could reveal broader implications for genome evolution and adaptation.

481 **Materials and methods**

482 **Strains, media, and growth conditions**

483 Strains characterized in this study are listed in Table S1. Strains were prepared for long-
484 term storage as 20% glycerol stocks at -80°C. Fresh cultures were revived and maintained on
485 YPD (1% yeast extract, 2% Bacto Peptone, 2% dextrose) agar medium, incubated at 30°C.
486 *Cryptococcus* transformants harboring dominant drug-resistance markers were selected on
487 YPD medium supplemented with 100 µg/mL nourseothricin (NAT), 200 µg/mL neomycin (G418),
488 or 100 µg/mL hygromycin B (HYG). Strains were grown in YPD liquid cultures at 30°C as
489 indicated. For plate growth assays, strains were cultivated on YPD, Murashige and Skoog (MS)
490 (Sigma-Aldrich M5519), or Niger seed (7% Niger seed, 0.1% dextrose). Sorbitol was added to
491 YPD medium at a 1 M concentration. To analyze cell growth in response to immunosuppressive
492 agents, rapamycin (100 ng/mL), FK506 (1 µg/mL), and cyclosporine A (100 µg/mL) were added
493 to YPD medium. For serial dilution assays, fresh cells were diluted to a starting OD_{600} of 0.1,
494 serially diluted 5-fold, and spotted onto plates for the indicated media and temperature
495 conditions. Plates were incubated for two to seven days and photographed daily. For capsule
496 analysis, strains were incubated for 3 days in RPMI media at 30˚C, followed by negative
497 staining with India ink. For mating assays, strains were incubated on MS plates, face up, in the
498 dark at room temperature for up to eight weeks. Spores dissected from MS plates were
499 germinated on YPD at 30°C for five days.

500

501 **Strain construction**

502 Mutant strains analyzed in this study were generated in the *C. neoformans* H99α,
503 YL99**a,** or KN99**a**/KN99α backgrounds. All genetic manipulations were done using CRISPR-
504 Cas9-mediated mutagenesis and the TRACE system, according to previously published
505 protocols [58, 59]. In brief, Cas9 was amplified from the pBHM2403 plasmid and gRNAs were
506 generated with sequence specific-primers and amplification of the gRNA scaffold from the

507 pBHM2329 plasmid [59]. Donor DNA templates for transformations were generated by PCR or
508 plasmid digestion and purified with the QIAquick gel extraction kit (Qiagen #28704). Cells and
509 DNA were prepared for transformation as described in the TRACE system, and electroporated
510 utilizing a BioRad gene pulser (0.45 kV, 125 μF, 600 Ω). Cells were recovered in YPD media for
511 2-3 hours at 30ºC following electroporation.

512 To generate the *PPG1* overexpression allele, the *TEF1* promoter (1.2 kb) and *PPG1*
513 coding regions were amplified from H99α genomic DNA and assembled into plasmid pSDMA57,
514 digested with XhoI and SpeI, via Gibson assembly (New England Biolabs E5510S) for targeting
515 to the safe haven (SH) locus [49]. GFP tagging of Nop1 was also performed through integration
516 at the safe haven. To facilitate homologous recombination at the target locus, the safe haven
517 plasmid pYSCE5 (pSH-P_{H3}-GFP-HYG) was designed to include a safe haven genomic
518 sequence containing AscI and PacI restriction sites for linearization, along with the histone H3
519 promoter, GFP, and the hygromycin B resistance gene (HYG). The *NOP1* gene, amplified from
520 H99α genomic DNA without its stop codon, was incorporated into plasmid pYSCE5 between the
521 *H3* promoter and GFP, generating pYSCE8 (pSH-H3-NOP1-GFP-HYG). Plasmids for targeted
522 integration at the safe haven were linearized via overnight digestion with AscI and PacI and gel-
523 purified prior to transformation. The *ppg1::NEO* deletion allele was made via PCR amplification
524 of approximately 1 kb homologous 5' and 3' flanking regions to the *PPG1* open reading frame,
525 which were then assembled with the neomycin resistance gene expression cassette (NEO)
526 through overlap PCR [60, 61]. Transformants were plated onto selective media (YPD+NEO or
527 YPD+HYG) and allowed to grow up to 7 days at 30ºC. Stable genomic integrants were verified
528 by diagnostic PCR amplifying the 5′ and 3′ flanking junctions of the insertion site.
529

530 **Primers, PCR genotyping, and RFLP analysis**

531 Primers employed in this study are listed in Table S2. Genomic DNA from strains
532 generated in this study was extracted from cells with the MasterPure Yeast DNA Purification Kit

533 (LGC Biosearch Technologies). Dissected progeny from mated crosses were genotyped by
534 colony PCR. Single colonies were picked into 0.25% SDS and 1 mM EDTA, briefly frozen at -
535 20 °C, and then heated at 100ºC for 10 minutes in a thermocycler. The resulting supernatants
536 were used as DNA templates for PCR. To determine the mating type of *C. neoformans* strains,
537 the *STE20* gene in the *MAT* locus was amplified using primers specific to the *STE20*α and
538 *STE20***a** alleles. The mitochondrial *COX1* gene, which differs in size in KN99 background strains
539 compared to H99 due to the presence of an intron, was probed to determine mitochondrial
540 inheritance. For KN99α *pph22*Δ *sup* crosses, the KN99**a** SSH118 strain, which has a
541 recombinant mitochondrial genome, was used as the wild-type parent to differentiate between
542 mitochondrial genotypes in the KN99 background progeny. After PCR amplification of *COX1*,
543 the resulting PCR product was digested with restriction enzyme BsrI for restriction fragment
544 length polymorphism (RFLP) analysis. Digestion of the *COX1* PCR product amplified from
545 KN99**a**, which contains three BsrI recognition sites, and SSH118, which has two BsrI sites, were
546 used as controls to determine the mitochondrial inheritance of the progeny from *pph22*Δ *sup* x
547 SSH118 crosses.
548
549 **Microscopy**
550 For sample preparation for scanning electron microscopy from mated strains of
551 *Cryptococcus*, an agar slice of the plated cells was fixed in a solution of 4% formaldehyde and
552 4% glutaraldehyde for 2 hours at 4°C. The fixed cells were then gradually dehydrated in a
553 graded ethanol series (30%, 50%, 70%, and 95%), with a 15-minute incubation at 4°C for each
554 concentration. This was followed by three washes with 100% ethanol, each for 15 minutes at
555 4°C. The samples were further dehydrated using a Ladd CPD3 Critical Point Dryer and coated
556 with a layer of gold using a Denton Desk V Sputter Coater (Denton Vacuum, USA). Hyphae,
557 basidia, and basidiospores were observed with a scanning electron microscope with an EDS
558 detector (Apreo S, ThermoFisher, USA). Brightfield, differential interference contrast (DIC), and

559 fluorescence microscopy images were visualized with an AxioScop 2 fluorescence microscope
560 and captured with an AxioCam MRm digital camera (Zeiss, Germany). Consistent exposure
561 times were used for all images captured from the same experiment. Image processing and
562 merging channels of fluorescent images was performed with ImageJ/Fiji software.
563
564 **Cell-cell fusion and mating assays**
565 To induce mating, the indicated strains were grown overnight in YPD medium, diluted to
566 an OD_{600} of 1.0, and 4 µL of each cell suspension was spotted onto MS agar plates. The plates
567 were incubated at room temperature in the dark and monitored for signs of filamentation and
568 sporulation for up to eight weeks. For wild-type mating crosses, *MAT***a** cells (KN99**a**) were mixed
569 with *MAT*α cells (H99α) in equal amounts and spotted onto MS plates. For crosses involving
570 *pph22*Δ and *far8*Δ strains, the following modifications were made to compensate for the
571 impaired growth of these mutants on MS medium. Fresh *pph22*Δ and *far8*Δ mutant cells were
572 first spotted onto MS agar and pre-incubated in the dark at room temperature for two days,
573 without the wild-type mating partner. After pre-growth, wild-type cells of the opposite mating type
574 were added directly on top of the mutant cells at a ten-fold lower cell amount. Twelve mating
575 spots were prepared per plate, with each spotted treated as an independent replicate. A wild-
576 type H99α x KN99**a** cross was included on each plate as a control. Basidiospores were
577 dissected from individual basidia, or randomly dissected, and incubated on YPD medium at
578 30ºC for 3 to 4 days to determine spore viability and germination rates.
579 To assess cell-cell fusion frequency in wild type x *pph22*Δ crosses, KN99**a** or KN99α
580 strains carrying a NEO resistance marker (JOHE10493, JOHE18842) were mixed in 1:10
581 proportions with *pph22*Δ*:NAT* **a** or α strains, spotted onto MS agar, and incubated in the dark at
582 room temperature for 3 days. A KN99**a***::NAT* (JOHE18853) x KN99α*::NEO* (JOHE18842) wild-
583 type cross was used as a control. The entire patch of cells was harvested and serially diluted in
584 PBS before plating onto YPD+NAT, YPD+NEO, and YPD+NAT+NEO selective media. Colony-

585 forming units (CFUs) were counted after incubation at 30°C for two days (for wild-type selection)
586 or four days (for pph22Δ and dual-resistant fusion products). Fusion frequency was calculated
587 as the number of CFUs on YPD+NAT+NEO divided by the total number of colonies on
588 YPD+NAT and YPD+NEO, and expressed as a percentage relative to the wild-type control.
589 Each assay was performed in triplicate.
590
591 **Whole-genome sequencing and SNP analysis**
592 Genomic DNA for whole-genome sequencing was extracted from saturated 4 mL YPD
593 cultures with the MasterPure Yeast DNA Purification Kit. The precipitated DNA was dissolved in
594 35 μL of 1x TE buffer (100 mM Tris-HCl, 10 mM EDTA, pH=8.0), and the concentration was
595 estimated using Qubit. Illumina sequencing was performed at the Duke Sequencing and
596 Genomic Technologies core facility (https://genome.duke.edu) with Novaseq X Plus, providing
597 250 bp paired-end reads. The Illumina sequences were trimmed using trim-galore (v 0.6.7) and
598 mapped to the H99α genome assembly (RefSeq: GCF_000149245.1) using Geneious software.
599 The resulting BAM files were converted to TDF format, and read coverage was visualized in IGV
600 to verify uniform read coverage across the genome**.** For SNP calling, the Illumina sequences
601 were mapped to the H99α genome assembly using the Geneious default mapper with five
602 iterations. Variant calling was performed with BAM mapped read files, with parameters set to a
603 0.9 variant frequency and a minimum of 100x coverage per variant. For the KN99**a**/KN99α
604 diploid strain (CnLC6683), variant calling was performed with a 0.45 frequency and 100x
605 coverage per variant. Illumina sequences from H99α and KN99**a**/KN99α served as controls for
606 SNP calling analysis. Variants were exported from Geneious as VCF files and imported into IGV
607 for visualization.
608
609
610

611 **Flow cytometry**

612 For ploidy determination of *Cryptococcus* samples, fluorescence activated cell sorting
613 (FACS) was performed according to a previously published protocol, with slight modifications
614 [62]. Wild-type and mutant strains were grown on YPD plate medium at 30ºC overnight,
615 harvested, and washed with PBS. The cells were then fixed in 70% ethanol for 16 hours at 4ºC.
616 Fixed cells were pelleted and washed with 1 mL NS buffer (10 mM Tris-HCl, 0.25 M sucrose, 1
617 mM EDTA, 1 mM $MgCl_2$, 0.1 mM $ZnCl_2$, 0.4 mM phenylmethylsulfonyl fluoride, and 7 mM β-
618 mercaptoethanol). After centrifugation, the cells were treated with RNase (0.5 mg/mL) and
619 stained with propidium iodide (10 µg/mL) in a 200 µL suspension of NS buffer for 2 hours in the
620 dark. Then, 50 µL of the stained cells were diluted into 200 µL of 50 mM Tris-HCl, pH=8.0, and
621 submitted to the Duke Cancer Institute Flow Cytometry Shared Resource for analysis.
622 Fluorescence was measured using a BD FACSCanto flow cytometer and analyzed with BD
623 FACSDiva software. Approximately 15,000 to 20,000 events were analyzed for each sample.
624

625 **Quantification and statistical analysis**

626 All statistical analyses and data visualizations were performed with GraphPad Prism v10
627 software. Details regarding replication, quantification, and statistical tests used for each
628 experiment are provided in the methods and corresponding figure legends.
629

630 **Acknowledgements**

631 PPP is supported by NIH/NIAID T32 grant AI052080-21 as a Tri-I MMPTP fellow. This
632 work is also supported by NIH/NIAID R01 grants AI039115-27, AI050113-20, and AI172451-03
633 awarded to JH. JH is a co-director of the CIFAR Fungal Kingdom: Threats & Opportunities
634 program. We thank Dr. Vikas Yadav for guidance and expertise and our laboratory manager
635 Anna Floyd Averette for technical support.

636 **References**

637 1. Goudreault M, D'Ambrosio LM, Kean MJ, Mullin MJ, Larsen BG, Sanchez A, et al. A
638 PP2A phosphatase high density interaction network identifies a novel striatin-interacting
639 phosphatase and kinase complex linked to the cerebral cavernous malformation 3
640 (CCM3) protein. Mol Cell Proteomics. 2009;8(1):157-71. Epub 2008/09/11. doi:
641 10.1074/mcp.M800266-MCP200. PubMed PMID: 18782753; PubMed Central PMCID:
642 2621004.
643 2. Neisch AL, Neufeld TP, Hays TS. A STRIPAK complex mediates axonal transport of
644 autophagosomes and dense core vesicles through PP2A regulation. J Cell Biol.
645 2017;216(2):441-61. Epub 2017/01/20. doi: 10.1083/jcb.201606082. PubMed PMID:
646 28100687; PubMed Central PMCID: PMC5294782.
647 3. Li D, Musante V, Zhou W, Picciotto MR, Nairn AC. Striatin-1 is a B subunit of protein
648 phosphatase PP2A that regulates dendritic arborization and spine development in
649 striatal neurons. J Biol Chem. 2018;293(28):11179-94. Epub 2018/05/29. doi:
650 10.1074/jbc.RA117.001519. PubMed PMID: 29802198; PubMed Central PMCID:
651 PMC6052221.
652 4. Gordon J, Hwang J, Carrier KJ, Jones CA, Kern QL, Moreno CS, et al. Protein
653 phosphatase 2a (PP2A) binds within the oligomerization domain of striatin and regulates
654 the phosphorylation and activation of the mammalian Ste20-Like kinase Mst3. BMC
655 Biochemistry. 2011;12:54. doi: 10.1186/1471-2091-12-54. PubMed PMID: 21985334;
656 PubMed Central PMCID: 3217859.
657 5. Janssens V, Goris J. Protein phosphatase 2A: a highly regulated family of
658 serine/threonine phosphatases implicated in cell growth and signalling. Biochem J.
659 2001;353(Pt 3):417-39. doi: 10.1042/0264-6021:3530417. PubMed PMID: 11171037;
660 PubMed Central PMCID: PMC1221586.
661 6. Cho US, Xu W. Crystal structure of a protein phosphatase 2A heterotrimeric
662 holoenzyme. Nature. 2007;445(7123):53-7. Epub 20061101. doi: 10.1038/nature05351.
663 PubMed PMID: 17086192.
664 7. Sandal P, Jong CJ, Merrill RA, Song J, Strack S. Protein phosphatase 2A - structure,
665 function and role in neurodevelopmental disorders. J Cell Sci. 2021;134(13). Epub
666 20210706. doi: 10.1242/jcs.248187. PubMed PMID: 34228795; PubMed Central PMCID:
667 PMC8277144.
668 8. Sents W, Ivanova E, Lambrecht C, Haesen D, Janssens V. The biogenesis of active
669 protein phosphatase 2A holoenzymes: a tightly regulated process creating phosphatase
670 specificity. FEBS J. 2013;280(2):644-61. Epub 20120425. doi: 10.1111/j.1742-
671 4658.2012.08579.x. PubMed PMID: 22443683.
672 9. Ribeiro PS, Josue F, Wepf A, Wehr MC, Rinner O, Kelly G, et al. Combined functional
673 genomic and proteomic approaches identify a PP2A complex as a negative regulator of
674 Hippo signaling. Mol Cell. 2010;39(4):521-34. Epub 2010/08/28. doi:
675 10.1016/j.molcel.2010.08.002. PubMed PMID: 20797625.
676 10. Kuck U, Radchenko D, Teichert I. STRIPAK, a highly conserved signaling complex,
677 controls multiple eukaryotic cellular and developmental processes and is linked with
678 human diseases. Biol Chem. 2019. Epub 2019/05/03. doi: 10.1515/hsz-2019-0173.
679 PubMed PMID: 31042639.
680 11. Kuck U, Poggeler S. STRIPAK, a fundamental signaling hub of eukaryotic development.
681 Microbiol Mol Biol Rev. 2024;88(4):e0020523. Epub 20241111. doi:
682 10.1128/mmbr.00205-23. PubMed PMID: 39526753; PubMed Central PMCID:
683 PMC11653735.
684 12. Jeong BC, Bae SJ, Ni L, Zhang X, Bai XC, Luo X. Cryo-EM structure of the Hippo
685 signaling integrator human STRIPAK. Nature Structural & Molecular Biology.

2021;28(3):290-9. Epub 2021/02/27. doi: 10.1038/s41594-021-00564-y. PubMed PMID: 33633399; PubMed Central PMCID: PMC8315899.

13. Shi Z, Jiao S, Zhou Z. STRIPAK complexes in cell signaling and cancer. Oncogene. 2016;35(35):4549-57. Epub 2016/02/16. doi: 10.1038/onc.2016.9. PubMed PMID: 26876214.

14. Bernhards Y, Poggeler S. The phocein homologue SmMOB3 is essential for vegetative cell fusion and sexual development in the filamentous ascomycete *Sordaria macrospora*. Curr Genet. 2011;57(2):133-49. Epub 20110113. doi: 10.1007/s00294-010-0333-z. PubMed PMID: 21229248; PubMed Central PMCID: PMC3059760.

15. Bloemendal S, Bernhards Y, Bartho K, Dettmann A, Voigt O, Teichert I, et al. A homologue of the human STRIPAK complex controls sexual development in fungi. Mol Microbiol. 2012;84(2):310-23. doi: 10.1111/j.1365-2958.2012.08024.x. PubMed PMID: 22375702.

16. Kuck U, Stein V. STRIPAK, a Key Regulator of Fungal Development, Operates as a Multifunctional Signaling Hub. J Fungi. 2021;7(6):443. Epub 2021/07/03. doi: 10.3390/jof7060443. PubMed PMID: 34206073; PubMed Central PMCID: PMC8226480.

17. Chen A, Liu N, Xu C, Wu S, Liu C, Qi H, et al. The STRIPAK complex orchestrates cell wall integrity signalling to govern the fungal development and virulence of *Fusarium graminearum*. Mol Plant Pathol. 2023;24(9):1139-53. Epub 20230606. doi: 10.1111/mpp.13359. PubMed PMID: 37278525; PubMed Central PMCID: PMC10423325.

18. Pracheil T, Thornton J, Liu Z. TORC2 signaling is antagonized by protein phosphatase 2A and the Far complex in *Saccharomyces cerevisiae*. Genetics. 2012;190(4):1325-39. doi: 10.1534/genetics.111.138305. PubMed PMID: 22298706; PubMed Central PMCID: 3316646.

19. Pracheil T, Liu Z. Tiered assembly of the yeast Far3-7-8-9-10-11 complex at the endoplasmic reticulum. J Biol Chem. 2013;288(23):16986-97. doi: 10.1074/jbc.M113.451674. PubMed PMID: 23625923; PubMed Central PMCID: 3675630.

20. Frost A, Elgort MG, Brandman O, Ives C, Collins SR, Miller-Vedam L, et al. Functional repurposing revealed by comparing *S. pombe* and *S. cerevisiae* genetic interactions. Cell. 2012;149(6):1339-52. doi: 10.1016/j.cell.2012.04.028. PubMed PMID: 22682253.

21. Poggeler S, Kuck U. A WD40 repeat protein regulates fungal cell differentiation and can be replaced functionally by the mammalian homologue striatin. Eukaryot Cell. 2004;3(1):232-40. doi: 10.1128/EC.3.1.232-240.2004. PubMed PMID: 14871953; PubMed Central PMCID: PMC329509.

22. Dettmann A, Heilig Y, Ludwig S, Schmitt K, Illgen J, Fleissner A, et al. HAM-2 and HAM-3 are central for the assembly of the *Neurospora* STRIPAK complex at the nuclear envelope and regulate nuclear accumulation of the MAP kinase MAK-1 in a MAK-2-dependent manner. Mol Microbiol. 2013;90(4):796-812. Epub 2013/09/14. doi: 10.1111/mmi.12399. PubMed PMID: 24028079.

23. Wang CL, Shim WB, Shaw BD. *Aspergillus nidulans* striatin (StrA) mediates sexual development and localizes to the endoplasmic reticulum. Fungal Genet Biol. 2010;47(10):789-99. Epub 20100626. doi: 10.1016/j.fgb.2010.06.007. PubMed PMID: 20601045.

24. Elramli N, Karahoda B, Sarikaya-Bayram O, Frawley D, Ulas M, Oakley CE, et al. Assembly of a heptameric STRIPAK complex is required for coordination of light-dependent multicellular fungal development with secondary metabolism in *Aspergillus nidulans*. PLoS Genet. 2019;15(3):e1008053. Epub 2019/03/19. doi: 10.1371/journal.pgen.1008053. PubMed PMID: 30883543; PubMed Central PMCID: PMC6438568.

25. Islam KT, Bond JP, Fakhoury AM. FvSTR1, a striatin orthologue in *Fusarium virguliforme*, is required for asexual development and virulence. Appl Microbiol Biotechnol. 2017;101(16):6431-45. Epub 2017/06/24. doi: 10.1007/s00253-017-8387-1. PubMed PMID: 28643182.
26. Yamamura Y, Shim WB. The coiled-coil protein-binding motif in *Fusarium verticillioides* Fsr1 is essential for maize stalk rot virulence. Microbiology. 2008;154(Pt 6):1637-45. doi: 10.1099/mic.0.2008/016782-0. PubMed PMID: 18524918.
27. Wang CL, Shim WB, Shaw BD. The *Colletotrichum graminicola* striatin orthologue Str1 is necessary for anastomosis and is a virulence factor. Mol Plant Pathol. 2016;17(6):931-42. Epub 20160218. doi: 10.1111/mpp.12339. PubMed PMID: 26576029; PubMed Central PMCID: PMC6638439.
28. Schmidpeter J, Dahl M, Hofmann J, Koch C. ChMob2 binds to ChCbk1 and promotes virulence and conidiation of the fungal pathogen *Colletotrichum higginsianum*. BMC Microbiol. 2017;17(1):22. Epub 20170119. doi: 10.1186/s12866-017-0932-7. PubMed PMID: 28103800; PubMed Central PMCID: PMC5248491.
29. Kim MS, Zhang H, Yan H, Yoon BJ, Shim WB. Characterizing co-expression networks underpinning maize stalk rot virulence in *Fusarium verticillioides* through computational subnetwork module analyses. Sci Rep. 2018;8(1):8310. Epub 20180529. doi: 10.1038/s41598-018-26505-2. PubMed PMID: 29844502; PubMed Central PMCID: PMC5974142.
30. Peterson PP, Choi JT, Fu C, Cowen LE, Sun S, Bahn YS, et al. The *Cryptococcus neoformans* STRIPAK complex controls genome stability, sexual development, and virulence. PLoS Pathog. 2024;20(11):e1012735. Epub 20241119. doi: 10.1371/journal.ppat.1012735. PubMed PMID: 39561188; PubMed Central PMCID: PMC11614259.
31. Giles SS, Dagenais TR, Botts MR, Keller NP, Hull CM. Elucidating the pathogenesis of spores from the human fungal pathogen *Cryptococcus neoformans*. Infect Immun. 2009;77(8):3491-500. Epub 20090518. doi: 10.1128/IAI.00334-09. PubMed PMID: 19451235; PubMed Central PMCID: PMC2715683.
32. Velagapudi R, Hsueh YP, Geunes-Boyer S, Wright JR, Heitman J. Spores as infectious propagules of *Cryptococcus neoformans*. Infect Immun. 2009;77(10):4345-55. Epub 2009/07/22. doi: 10.1128/IAI.00542-09. PubMed PMID: 19620339; PubMed Central PMCID: PMC2747963.
33. Kwon-Chung KJ, Edman JC, Wickes BL. Genetic association of mating types and virulence in *Cryptococcus neoformans*. Infect Immun. 1992;60(2):602-5. doi: 10.1128/iai.60.2.602-605.1992. PubMed PMID: 1730495; PubMed Central PMCID: PMC257671.
34. Zhao Y, Lin J, Fan Y, Lin X. Life Cycle of *Cryptococcus neoformans*. Annu Rev Microbiol. 2019;73:17-42. Epub 20190513. doi: 10.1146/annurev-micro-020518-120210. PubMed PMID: 31082304.
35. Sun S, Coelho MA, David-Palma M, Priest SJ, Heitman J. The evolution of sexual reproduction and the mating-type locus: links to pathogenesis of *Cryptococcus* human pathogenic fungi. Annu Rev Genet. 2019;53:417-44. Epub 2019/09/21. doi: 10.1146/annurev-genet-120116-024755. PubMed PMID: 31537103; PubMed Central PMCID: PMC7025156.
36. Hull CM, Heitman J. Genetics of *Cryptococcus neoformans*. Annu Rev Genet. 2002;36:557-615. Epub 2002/11/14. doi: 10.1146/annurev.genet.36.052402.152652. PubMed PMID: 12429703.
37. Idnurm A. A tetrad analysis of the basidiomycete fungus *Cryptococcus neoformans*. Genetics. 2010;185(1):153-63. Epub 20100215. doi: 10.1534/genetics.109.113027. PubMed PMID: 20157004; PubMed Central PMCID: PMC2870951.

38. Yadav V, Sun S, Heitman J. Uniparental nuclear inheritance following bisexual mating in fungi. eLife. 2021;10. Epub 2021/08/03. doi: 10.7554/eLife.66234. PubMed PMID: 34338631; PubMed Central PMCID: PMC8412948.
39. Yan Z, Xu J. Mitochondria are inherited from the *MAT*a parent in crosses of the basidiomycete fungus *Cryptococcus neoformans*. Genetics. 2003;163(4):1315-25. doi: 10.1093/genetics/163.4.1315. PubMed PMID: 12702677; PubMed Central PMCID: PMC1462512.
40. Lavanchy G, Schwander T. Hybridogenesis. Curr Biol. 2019;29(3):539. doi: 10.1016/j.cub.2019.01.020. PubMed PMID: 30721675.
41. Casselton LA, Olesnicky NS. Molecular genetics of mating recognition in basidiomycete fungi. Microbiol Mol Biol Rev. 1998;62(1):55-70. doi: 10.1128/MMBR.62.1.55-70.1998. PubMed PMID: 9529887; PubMed Central PMCID: PMC98906.
42. Kozubowski L, Heitman J. Septins enforce morphogenetic events during sexual reproduction and contribute to virulence of *Cryptococcus neoformans*. Mol Microbiol. 2010;75(3):658-75. Epub 2009/12/01. doi: 10.1111/j.1365-2958.2009.06983.x. PubMed PMID: 19943902; PubMed Central PMCID: PMC3699866.
43. Lin X, Hull CM, Heitman J. Sexual reproduction between partners of the same mating type in *Cryptococcus neoformans*. Nature. 2005;434(7036):1017-21. Epub 2005/04/23. doi: 10.1038/nature03448. PubMed PMID: 15846346.
44. Xu J, Ali RY, Gregory DA, Amick D, Lambert SE, Yoell HJ, et al. Uniparental mitochondrial transmission in sexual crosses in *Cryptococcus neoformans*. Curr Microbiol. 2000;40(4):269-73. doi: 10.1007/s002849910053. PubMed PMID: 10688697.
45. Matha AR, Lin X. Current perspectives on uniparental mitochondrial inheritance in *Cryptococcus neoformans*. Pathogens. 2020;9(9). Epub 20200910. doi: 10.3390/pathogens9090743. PubMed PMID: 32927641; PubMed Central PMCID: PMC7559238.
46. Nielsen K, Cox GM, Wang P, Toffaletti DL, Perfect JR, Heitman J. Sexual cycle of *Cryptococcus neoformans* var. *grubii* and virulence of congenic a and alpha isolates. Infect Immun. 2003;71(9):4831-41. Epub 2003/08/23. doi: 10.1128/IAI.71.9.4831-4841.2003. PubMed PMID: 12933823; PubMed Central PMCID: PMC187335.
47. Janbon G, Ormerod KL, Paulet D, Byrnes EJ, 3rd, Yadav V, Chatterjee G, et al. Analysis of the genome and transcriptome of *Cryptococcus neoformans* var. *grubii* reveals complex RNA expression and microevolution leading to virulence attenuation. PLoS Genet. 2014;10(4):e1004261. Epub 2014/04/20. doi: 10.1371/journal.pgen.1004261. PubMed PMID: 24743168; PubMed Central PMCID: PMC3990503.
48. Arras SDM, Ormerod KL, Erpf PE, Espinosa MI, Carpenter AC, Blundell RD, et al. Convergent microevolution of *Cryptococcus neoformans* hypervirulence in the laboratory and the clinic. Sci Rep. 2017;7(1):17918. Epub 20171220. doi: 10.1038/s41598-017-18106-2. PubMed PMID: 29263343; PubMed Central PMCID: PMC5738413.
49. Arras SD, Chitty JL, Blake KL, Schulz BL, Fraser JA. A genomic safe haven for mutant complementation in *Cryptococcus neoformans*. PLoS One. 2015;10(4):e0122916. Epub 20150409. doi: 10.1371/journal.pone.0122916. PubMed PMID: 25856300; PubMed Central PMCID: PMC4391909.
50. Abramson J, Adler J, Dunger J, Evans R, Green T, Pritzel A, et al. Accurate structure prediction of biomolecular interactions with AlphaFold 3. Nature. 2024;630(8016):493-500. Epub 20240508. doi: 10.1038/s41586-024-07487-w. PubMed PMID: 38718835; PubMed Central PMCID: PMC11168924.
51. Mirdita M, Schütze K, Moriwaki Y, Heo L, Ovchinnikov S, Steinegger M. ColabFold: Making Protein folding accessible to all. Nature Methods. 2022. doi: 10.1038/s41592-022-01488-1.

52. Yadav V, Sun S, Heitman J. On the evolution of variation in sexual reproduction through the prism of eukaryotic microbes. Proc Natl Acad Sci U S A. 2023;120(10):e2219120120. Epub 20230303. doi: 10.1073/pnas.2219120120. PubMed PMID: 36867686; PubMed Central PMCID: PMC10013875.
53. Fu C, Sun S, Billmyre RB, Roach KC, Heitman J. Unisexual versus bisexual mating in *Cryptococcus neoformans*: Consequences and biological impacts. Fungal Genet Biol. 2015;78:65-75. Epub 2014/09/01. doi: 10.1016/j.fgb.2014.08.008. PubMed PMID: 25173822; PubMed Central PMCID: PMC4344436.
54. Sakuma C, Saito Y, Umehara T, Kamimura K, Maeda N, Mosca TJ, et al. The Strip-Hippo pathway regulates synaptic terminal formation by modulating actin organization at the *Drosophila* neuromuscular synapses. Cell reports. 2016;16(9):2289-97. Epub 2016/08/23. doi: 10.1016/j.celrep.2016.07.066. PubMed PMID: 27545887; PubMed Central PMCID: PMC5023852.
55. Gupta R, Kumar G, Jain BP, Chandra S, Goswami SK. Ectopic expression of 35 kDa and knocking down of 78 kDa SG2NAs induce cytoskeletal reorganization, alter membrane sialylation, and modulate the markers of EMT. Mol Cell Biochem. 2021;476(2):633-48. Epub 2020/10/22. doi: 10.1007/s11010-020-03932-2. PubMed PMID: 33083950.
56. Wernet V, Wackerle J, Fischer R. The STRIPAK component SipC is involved in morphology and cell-fate determination in the nematode-trapping fungus *Duddingtonia flagrans*. Genetics. 2022;220(1). Epub 2021/12/02. doi: 10.1093/genetics/iyab153. PubMed PMID: 34849851; PubMed Central PMCID: PMC8733638.
57. Jacinto E, Loewith R, Schmidt A, Lin S, Ruegg MA, Hall A, et al. Mammalian TOR complex 2 controls the actin cytoskeleton and is rapamycin insensitive. Nat Cell Biol. 2004;6(11):1122-8. PubMed PMID: 15467718.
58. Fan Y, Lin X. Multiple applications of a transient CRISPR-Cas9 coupled with electroporation (TRACE) system in the *Cryptococcus neoformans* species complex. Genetics. 2018;208(4):1357-72. Epub 20180214. doi: 10.1534/genetics.117.300656. PubMed PMID: 29444806; PubMed Central PMCID: PMC5887135.
59. Huang MY, Joshi MB, Boucher MJ, Lee S, Loza LC, Gaylord EA, et al. Short homology-directed repair using optimized Cas9 in the pathogen *Cryptococcus neoformans* enables rapid gene deletion and tagging. Genetics. 2022;220(1). doi: 10.1093/genetics/iyab180. PubMed PMID: 34791226; PubMed Central PMCID: PMC8733451.
60. Lin X, Chacko N, Wang L, Pavuluri Y. Generation of stable mutants and targeted gene deletion strains in *Cryptococcus neoformans* through electroporation. Med Mycol. 2015;53(3):225-34. Epub 20141224. doi: 10.1093/mmy/myu083. PubMed PMID: 25541555; PubMed Central PMCID: PMC4574871.
61. Davidson RC, Cruz MC, Sia RA, Allen B, Alspaugh JA, Heitman J. Gene disruption by biolistic transformation in serotype D strains of *Cryptococcus neoformans*. Fungal Genet Biol. 2000;29(1):38-48. Epub 2000/04/26. doi: 10.1006/fgbi.1999.1180. PubMed PMID: 10779398.
62. Tanaka R, Taguchi H, Takeo K, Miyaji M, Nishimura K. Determination of ploidy in *Cryptococcus neoformans* by flow cytometry. J Med Vet Mycol. 1996;34(5):299-301. PubMed PMID: 8912162.

883 **Figure legends**

884 **Figure 1.** *pph22*Δ x wild type crosses exhibit unusual sexual development. A) Mating efficiency
885 of *pph22*Δ strains crossed with wild-type of the opposite mating type (H99α or KN99**a**). Images
886 were taken between 4 to 6 weeks of incubation on MS plates. Scale bars in the middle and
887 bottom panels are 200 μm and 20 μm, respectively. B) Scanning electron microscopy (SEM) of
888 sexual structures in WT x WT and *pph22*Δ x WT crosses showing examples of a hyphal filament
889 terminating in a basidial head and basidiospores emerging from a basidium. The clamp cells
890 (white arrowheads) in the wild-type cross are fused to the subapical cell in the elongating hypha.
891 In *pph22*Δ x WT crosses, both fused and unfused clamp cells were often observed along the
892 same hypha. Scale bars in each panel represent 5 μm.

893

894 **Figure 2.** Progeny from *pph22*Δ x wild type exhibit uniparental nuclear inheritance from H99α
895 and lack evidence of meiotic recombination. Whole-genome sequencing followed by SNP
896 analysis revealed no contribution of the KN99**a** *pph22*Δ parental genome, as evidenced by the
897 absence of SNPs compared to the H99α reference genome. The three known polymorphic
898 regions distinguishing H99 and KN99 background strains are located on chromosomes 5 (the
899 mating-type locus), 11, and 14. These regions are highlighted in the lower panels, with the
900 chromosomal coordinates labeled accordingly. The KN99**a**/KN99α diploid strain (CnLC6683),
901 from which KN99**a** *pph22*Δ was obtained, was used as a control for variant calling. The few
902 SNPs identified in the progeny were restricted to nucleotide repeat regions. Mitochondrial
903 haplotypes were determined based on the presence or absence of an intron in the *COX1* gene
904 from whole-genome sequencing reads. “Germ.” stands for the germination frequency of the
905 indicated basidium and “P” stands for progeny.

906

907 **Figure 3.** Fluorescence microscopy depicts loss of one parental nucleus following hyphal
908 branching during pseudosexual reproduction. A) Loss of the wild-type nucleus at a hyphal
909 branch point in *pph22*Δ Nop1-GFP x WT Nop1-RFP. B) and C) Inheritance of only the *pph22*Δ
910 nucleus in basidiospores, which appear collapsed on the basidial head and have an irregular
911 morphology, is observed after loss of the WT nucleus in a hyphal compartment (B) and following
912 branching (C). D) Loss of the wild-type nucleus and retention of the *pph22*Δ nucleus results in
913 severely abnormal hyphal development (white arrowhead). In another hyphal branch, both
914 nuclei have undergone division in the dikaryon without segregating into separate hyphal cells
915 (grey arrowheads). The white arrowheads indicate the point in the hypha where one parental
916 nucleus is lost. The scale bar in each panel represents 5 µm.

917

918 **Figure 4.** The *pph22*Δ *suppressor* strains can restore α-**a** sexual mating in crosses with wild
919 type. A) Mating efficiencies in wild-type and *pph22*Δ *sup* crosses. Hyphal production and
920 elongation, and sporulation were observed to similar extents. B) Germination of spores
921 dissected from *pph22*Δ *sup* x WT after two days of incubation on YPD. Each row depicts spores
922 from separate basidia. Colonies that grew on YPD+NAT (containing the *pph22*Δ*::NAT* mutant
923 allele) are indicated by the white boxes. C) Genotyping analysis of progeny dissected from
924 *pph22*Δ *sup* strains crossed with the KN99**a** strain bearing recombinant mitochondria (SSH118).
925 Each spot is from a separate mating patch and is considered an independent experiment.

926

927 **Figure 5.** Overexpression of *PPG1* suppresses the *pph22*Δ mutation. A) Germination of spores
928 dissected from a *PPH22/pph22*Δ heterozygous mutant diploid strain expressing *TEF1-PPG1*
929 (*PPG1-OE)* on YPD. The genotypes of the colonies indicated were determined from growth on
930 YPD+NAT (*pph22*Δ::*NAT* allele) and YPD+NAT+NEO (*pph22*Δ*::NAT* and P_{TEF1}*-PPG1-NEO*

931 alleles). B) The indicated strains were serially diluted and grown on YPD solid media at 25ºC,
932 30ºC, and 37ºC; or YPD supplemented with 1 M sorbitol, 100 ng/mL rapamycin, 1 µg/mL FK506,
933 or 100 µg/mL cyclosporine A, each at 30ºC. Images were taken after three days incubation. C)
934 Strains were grown in liquid culture overnight in YPD at 30ºC and plated onto Niger seed agar.
935 Images were captured after four days. D) Analysis of capsule formation by India ink staining.
936 The indicated strains were grown for 3 days in RPMI media at 30ºC. Images are representative
937 of two biological replicates. Scale bar is 5 µm. E) Mating of *ppg1*Δ and *pph22*Δ *PPG1-OE*
938 strains crossed to wild type on MS media. Images were taken after six weeks. White
939 arrowheads indicate bald basidia heads that did not produce spores. The scale bars in the
940 middle and bottom panels are 200 µm and 50 µm.

941

942 **Figure 6.** *far8*Δ mutants also display a high rate of pseudosexual reproduction. A) SEM of
943 mated wild-type and *far8*Δ shows two basidia heads producing spores with abnormal
944 morphology. In the basidium on the right, spores are seen budding from seven independent
945 spots on the basidial head. The scale bar represents 5 µm. B) Dissection of spores from *far8*Δ x
946 WT yields colonies mostly homogenous in size on YPD. *far8*Δ mutants were identified based on
947 growth on YPD+NEO and form smaller, slow-growing colonies compared to wild type. Each row
948 of spores is from an independent basidium. C) Genotyping analysis of progeny from individual
949 basidia in *far8*Δ x WT crosses. Each spot analyzed is from an independent mating experiment.

950

Figure 1

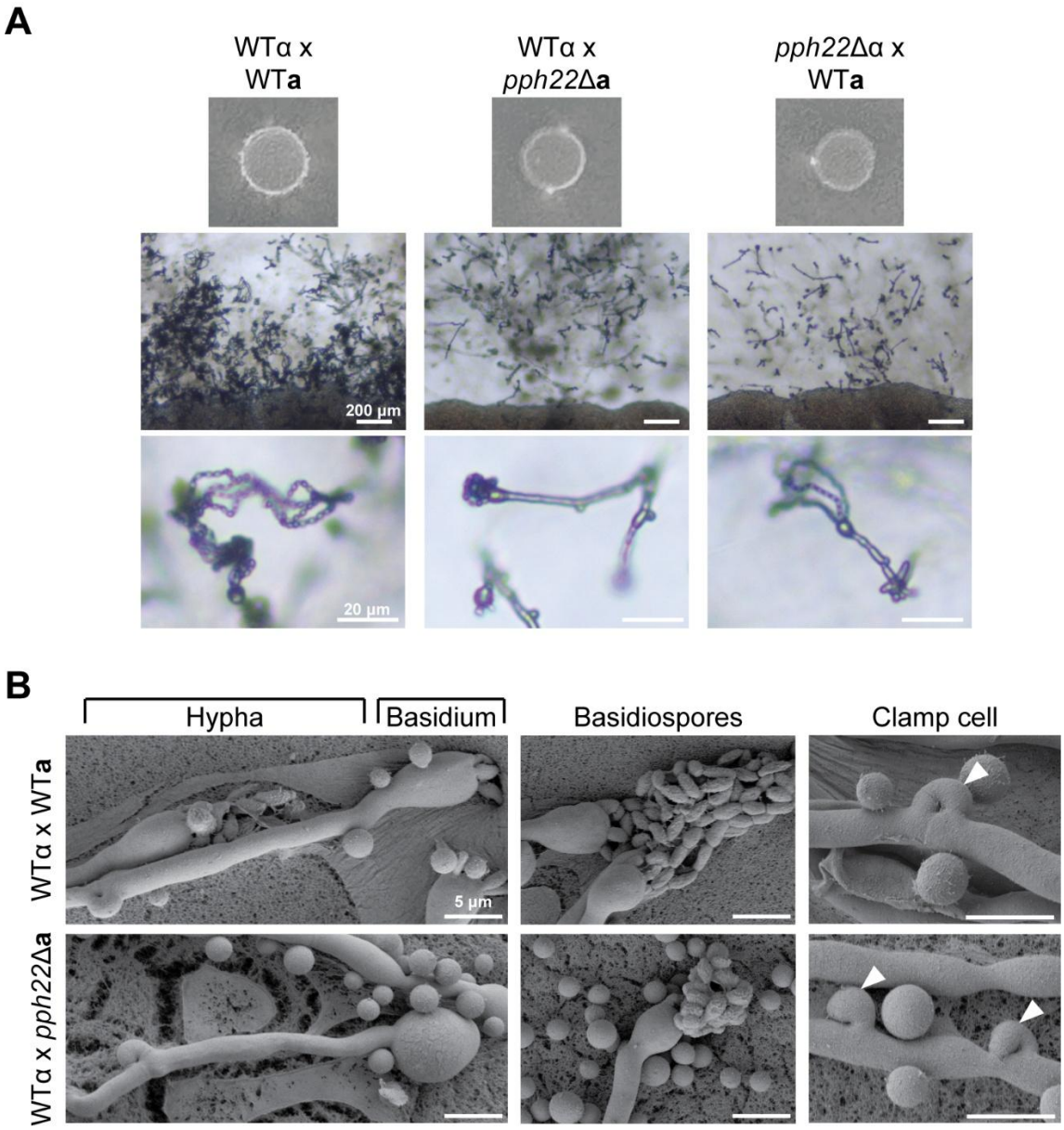
A
WTα x
WTa
WTα x
pph22Δa
pph22Δα x
WTa
200 µm
20 µm
B
Hypha
Basidium
Basidiospores
Clamp cell
WTα x WTa
WTα x pph22Δa
5 µm

Table 1. Genotyping analysis of spores from individual basidia and from random spore dissection in *pph22*Δ x wild type crosses. Spot refers to the individual mating spot from which those basidia were dissected in the indicated crosses, with each spot being an independent experiment. Mito. refers to mitochondria.

Spot	Basidia #	Spores germinated/dissected	% Germination	NAT^R	*MAT*	Mito.
pph22Δ::NAT **a** (PP56) x H99α						
A	1	13/14	93	0	All α	**a**
	2	1/14	7	0	All α	**a**
	3	13/14	93	0	All α	**a**
	4	3/9	33	0	All α	**a**
	5	14/14	100	0	All α	**a**
B	6	14/28	50	0	All α	α
	7	26/28	93	0	All α	α
	8	10/16	63	0	All α	α
	9	16/23	70	0	All α	α
	10	27/27	100	0	All α	α
	11	13/14	93	0	All α	α
C	12	11/14	79	0	All α	**a**
	13	13/14	93	0	All α	**a**
	14	14/14	100	0	All α	**a**
pph22Δ::NAT **a** (PP58) x H99α						
D	1	12/14	86	0	All α	**a**
	2	14/14	100	0	All α	α
	3	14/14	100	0	All α	**a**
	4	13/14	93	0	All α	**a**
	5	11/14	79	0	All α	**a**
E	6	13/14	93	0	All α	**a**
	7	14/14	100	0	All α	**a**
	8	3/9	33	0	All α	**a**
pph22Δ::NAT α (PP53) x KN99**a**						
F	1	26/28	93	0	All a	**a**
	2	8/18	44	0	All **a**	**a**
	3	18/28	64	0	All **a**	**a**
	4	16/17	94	0	All **a**	**a**
	5	18/22	82	0	All **a**	**a**
	6	26/50	52	0	All **a**	**a**

Random spore dissection

Spot	Spore #	NAT^R	*MAT*	Mito.
pph22Δ::NAT **a** (PP58) x H99α				
G	1-50	0	All α	**a**
H	51-65	0	All α	α

Figure 2

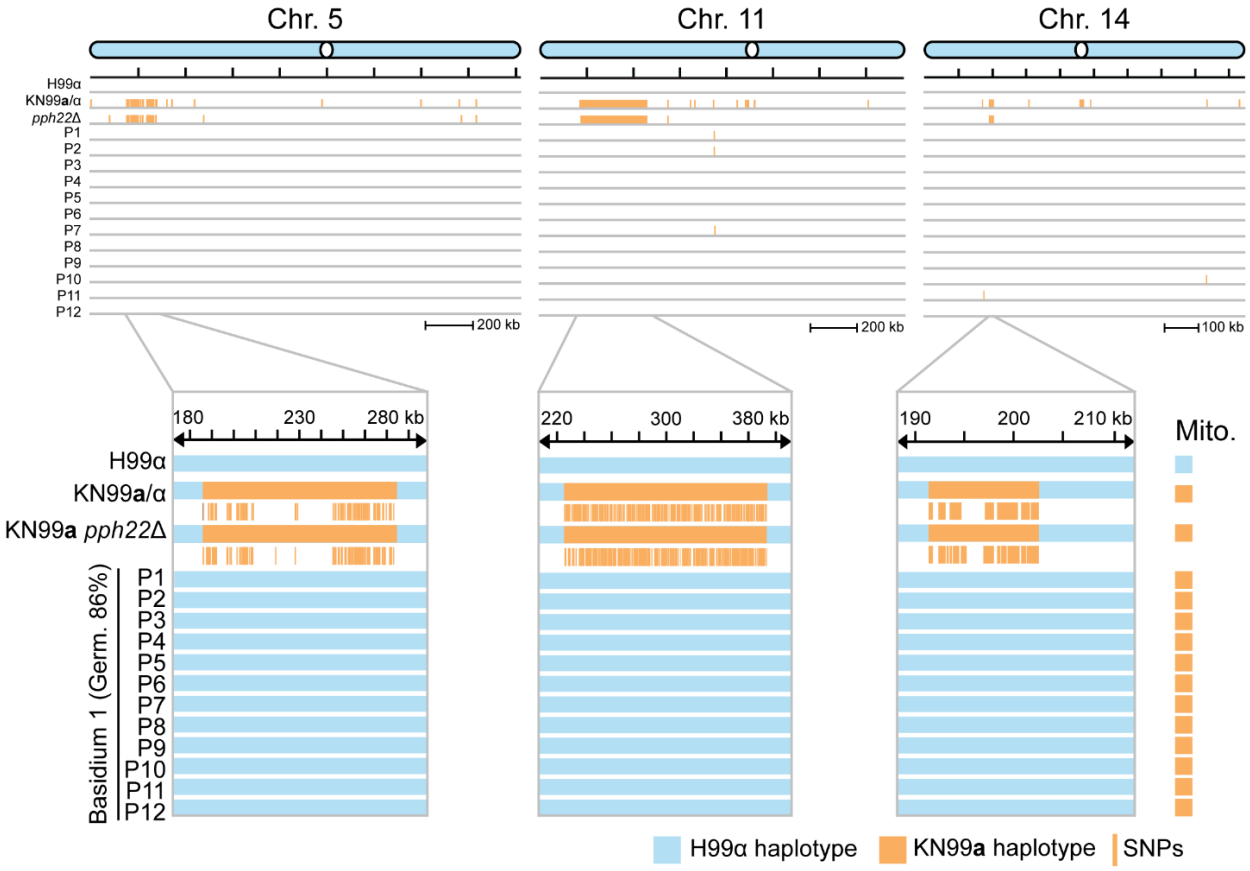
Chr. 5
Chr. 11
Chr. 14
H99α
KN99a/α
pph22Δ
P1
P2
P3
P4
P5
P6
P7
P8
P9
P10
P11
P12
200 kb
200 kb
100 kb
180
230
280 kb
220
300
380 kb
190
200
210 kb
Mito.
H99α
KN99a/α
KN99a pph22Δ
Basidium 1 (Germ. 86%)
H99α haplotype
KN99a haplotype
SNPs

Figure 3

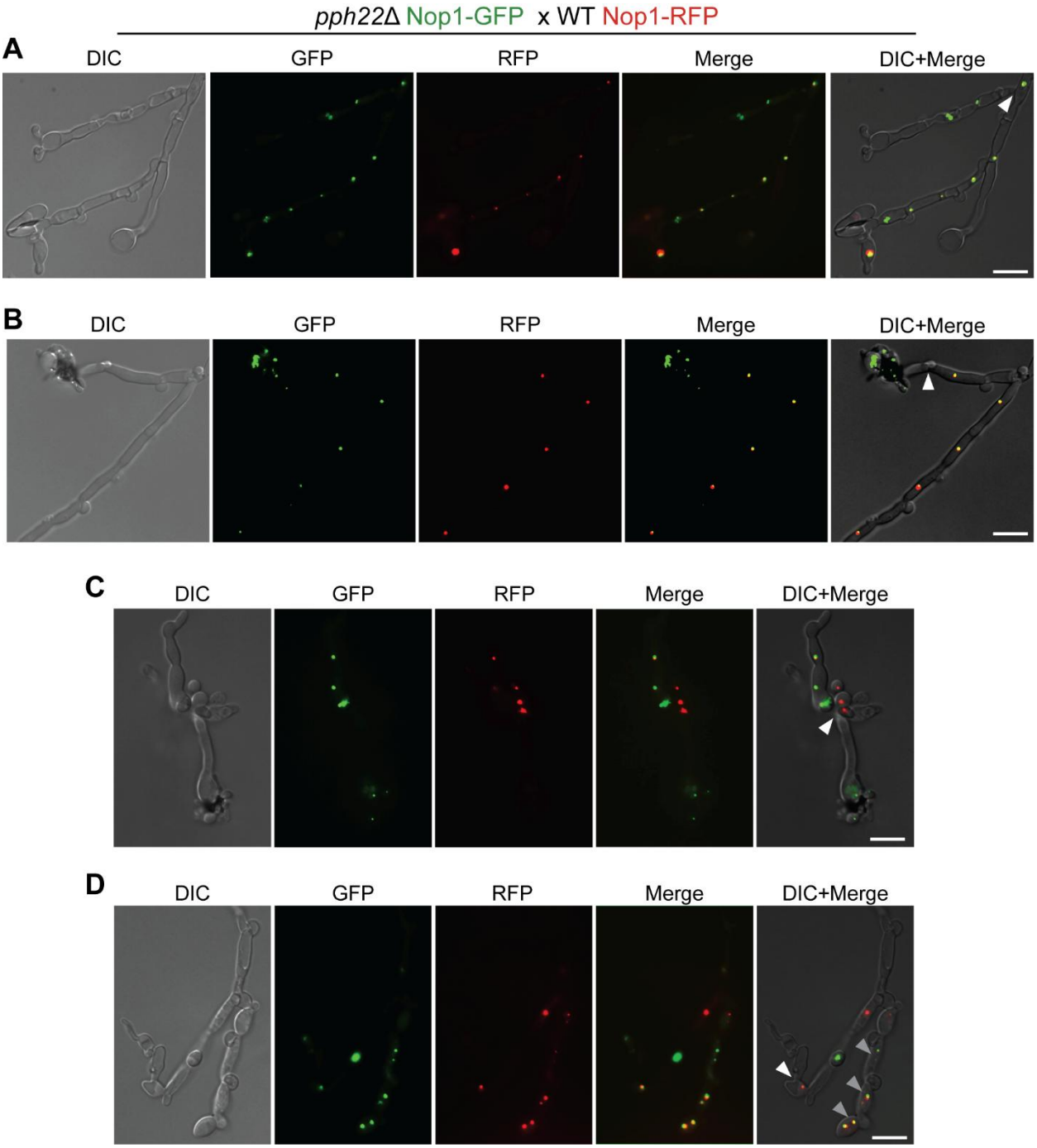
*pph22*Δ Nop1-GFP x WT Nop1-RFP
A
DIC
GFP
RFP
Merge
DIC+Merge
B
DIC
GFP
RFP
Merge
DIC+Merge
C
DIC
GFP
RFP
Merge
DIC+Merge
D
DIC
GFP
RFP
Merge
DIC+Merge

Figure 4

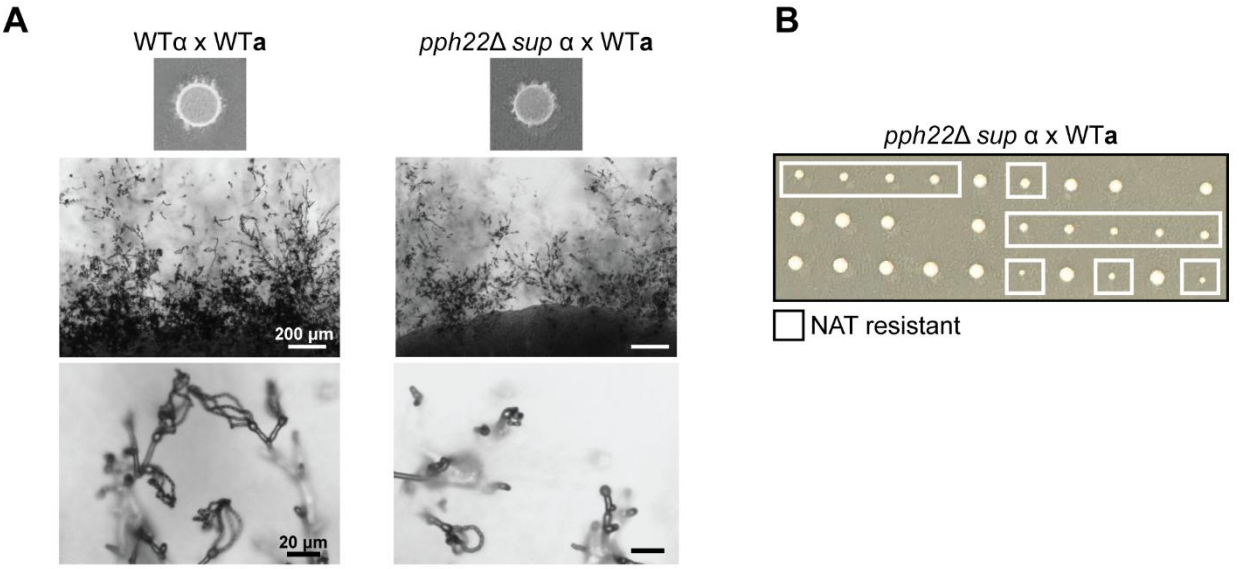

C

Spot	Basidia #	Spores germinated/dissected	% Germination	NAT^R	*MAT*	Mito.
pph22Δ::NAT sup α (PP84) x KN99**a** (SSH118)						
A	1	12/12	100	7	4 **a**, 8 α/**a**	**a**
B	2	8/14	57	6	2 **a**, 6 α/**a**	**a**
C	3	11/14	79	7	5 **a**, 6 α/**a**	**a**
D	4	13/14	93	6	5 **a**, 8 α/**a**	**a**
E	5	14/14	100	3	6 **a**, 8 α/**a**	**a**
F	6	9/14	64	3	4 **a**, 5 α/**a**	**a**
G	7	13/14	93	4	8 **a**, 5 α/**a**	**a**
pph22Δ::NAT sup α (PP80) x KN99**a** (SSH118)						
A	1	8/9	89	0	8 **a**	**a**
B	2	10/14	71	0	10 **a**	**a**
C	3	10/14	71	0	10 **a**	**a**
D	4	13/14	93	0	13 **a**	**a**
E	5	10/10	100	0	10 **a**	**a**
F	6	12/12	100	0	12 **a**	**a**
G	7	13/14	93	0	13 **a**	**a**
H	8	13/14	93	0	13 **a**	**a**
I	9	10/10	100	0	10 **a**	**a**
J	10	14/14	100	0	14 **a**	**a**
K	11	14/14	100	0	14 **a**	**a**
L	12	7/7	100	0	7 **a**	**a**

Figure 5

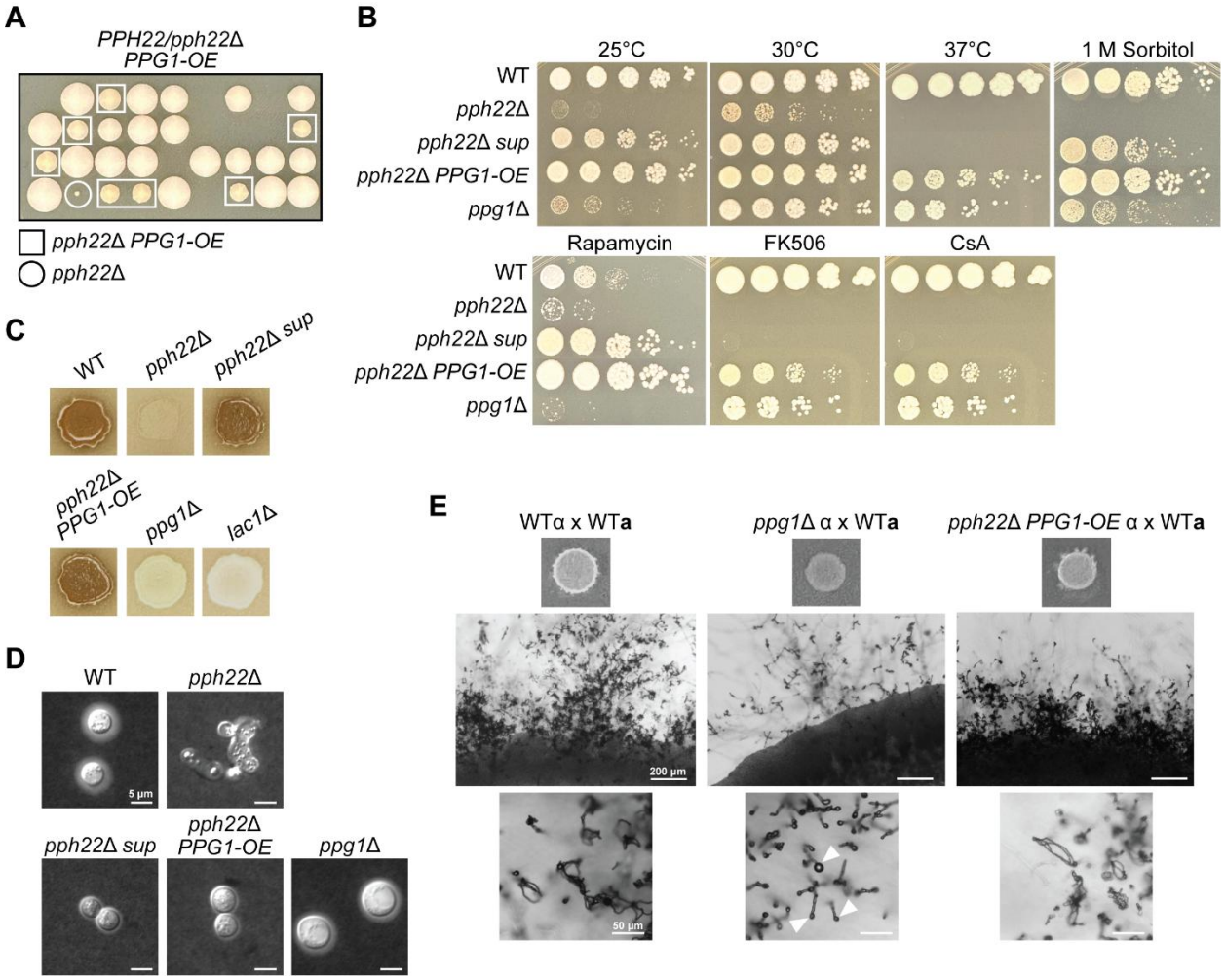
A
PPH22/pph22Δ
PPG1-OE
pph22Δ PPG1-OE
pph22Δ
B
25°C
30°C
37°C
1 M Sorbitol
WT
pph22Δ
pph22Δ sup
pph22Δ PPG1-OE
ppg1Δ
Rapamycin
FK506
CsA
C
WT
pph22Δ
pph22Δ sup
pph22Δ PPG1-OE
ppg1Δ
lac1Δ
D
WT
pph22Δ
5 µm
pph22Δ sup
pph22Δ PPG1-OE
ppg1Δ
E
WTα x WTa
ppg1Δ α x WTa
pph22Δ PPG1-OE α x WTa
200 µm
50 µm

Figure 6

A

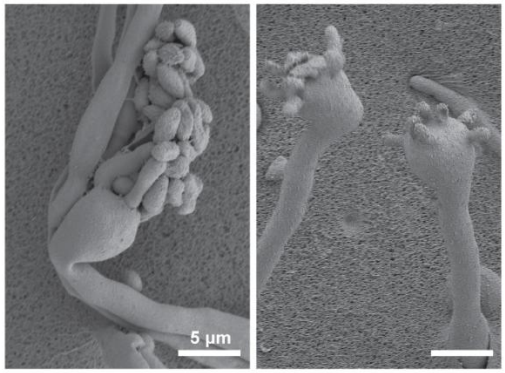

B

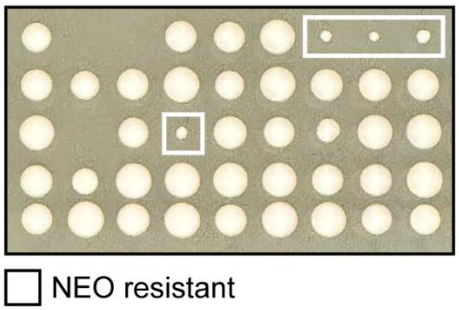

C

Spot	Basidia #	Spores germinated/ dissected	% Germination	NEO^R/ NAT^R	*MAT*	Mito.
far8Δ::NEO **a** (YSB11129) x H99α						
A	1	12/14	86	0	All α	**a**
	2	14/14	100	0	11 α, 3 α/**a**	**a**
B	3	13/20	65	12	5 **a**, 7 α, 1 α/**a**	**a**
C	4	3/5	60	2	1 **a**, 1 α, 1 α/**a**	**a**
	5	6/14	43	6	2 **a**, 1 α, 3 α/**a**	**a**
far8Δ::NEO **a** (YSB11132) x H99α						
D	1	12/13	92	0	All α	**a**
	2	8/13	62	0	All α	**a**
E	3	14/14	100	0	All α	**a**
	4	13/14	93	0	All α	**a**
F	5	9/14	64	0	All α	**a**
	6	18/18	100	0	All α	**a**
far8Δ::NAT α (YSB9100) x KN99**a**						
G	1	9/14	64	0	All **a**	**a**
	2	12/13	92	0	All **a**	**a**
H	3	12/14	86	0	All **a**	**a**
I	4	12/14	86	0	All **a**	**a**
	5	10/14	71	7	2 α, 8 α/**a**	**a**